Chem Soc Rev

REVIEW ARTICLE

View Article Online
View Journal | View Issue

Cite this: *Chem. Soc. Rev.*, 2017, **46**, 1730

Colloidal metal oxide nanocrystals as charge transporting layers for solution-processed light-emitting diodes and solar cells

Xiaoyong Liang,†[a] Sai Bai,†[b] Xin Wang,[a] Xingliang Dai,[a] Feng Gao,[b] Baoquan Sun,[c] Zhijun Ning,[d] Zhizhen Ye*[a] and Yizheng Jin*[e]

Colloidal metal oxide nanocrystals offer a unique combination of excellent low-temperature solution processability, rich and tuneable optoelectronic properties and intrinsic stability, which makes them an ideal class of materials as charge transporting layers in solution-processed light-emitting diodes and solar cells. Developing new material chemistry and custom-tailoring processing and properties of charge transporting layers based on oxide nanocrystals hold the key to boosting the efficiency and lifetime of all-solution-processed light-emitting diodes and solar cells, and thereby realizing an unprecedented generation of high-performance, low-cost, large-area and flexible optoelectronic devices. This review aims to bridge two research fields, chemistry of colloidal oxide nanocrystals and interfacial engineering of optoelectronic devices, focusing on the relationship between chemistry of colloidal oxide nanocrystals, processing and properties of charge transporting layers and device performance. Synthetic chemistry of colloidal oxide nanocrystals, ligand chemistry that may be applied to colloidal oxide nanocrystals and chemistry associated with post-deposition treatments are discussed to highlight the ability of optimizing processing and optoelectronic properties of charge transporting layers. Selected examples of solution-processed solar cells and light-emitting diodes with oxide-nanocrystal charge transporting layers are examined. The emphasis is placed on the correlation between the properties of oxide-nanocrystal charge transporting layers and device performance. Finally, three major challenges that need to be addressed in the future are outlined. We anticipate that this review will spur new material design and simulate new chemistry for colloidal oxide nanocrystals, leading to charge transporting layers and solution-processed optoelectronic devices beyond the state-of-the-art.

Received 17th February 2016

DOI: 10.1039/c6cs00122j

rsc.li/chem-soc-rev

1. Introduction

The exciting discoveries and tremendous progress of material chemistry create families of solution-processed semiconductors, including conjugated polymers,[1,2] colloidal quantum dots (QDs)[3–5] and organic–inorganic hybrid lead–halide hybrid perovskites.[6,7] These materials with intriguing optoelectronic properties can be processed as thin films by high-throughput and vacuum-free printing and coating techniques, such as inkjet-printing, roll-to-roll printing and blade-coating.[8–16] Many printing and coating procedures can be completed at low temperatures. Therefore, they are compatible with flexible and light-weight plastic substrates. These merits promise an unprecedented generation of low-cost, large-area and flexible light-emitting diodes (LEDs) and solar cells processed by solution-based techniques.

High-performance LEDs and solar cells are no doubt the results of extraordinary cooperation of multiple functional components. For the state-of-the-art solution-processed LEDs or solar cells, charge transporting layers (CTLs), *i.e.* electron transporting layers (ETLs) and hole transporting layers (HTLs), are essential components (Fig. 1). CTLs affect not only charge injection (or extraction) into (or out of) the active layers, but also many other elementary physical processes for device operation, such as interfacial charge recombination and light extraction (or light absorption) in LEDs (or solar cells). The integration of

[a] *State Key Laboratory of Silicon Materials, School of Materials Science and Engineering, Zhejiang University, Hangzhou 310027, People's Republic of China. E-mail: yezz@zju.edu.cn*
[b] *Department of Physics, Chemistry and Biology (IFM), Linköping University, SE-581 83 Linköping, Sweden*
[c] *Jiangsu Key Laboratory for Carbon-Based Functional Materials & Devices, Institute of Functional Nano & Soft Materials (FUNSOM), Soochow University, Suzhou 215123, People's Republic of China*
[d] *Shanghai Tech University, China*
[e] *Center for Chemistry of High-Performance & Novel Materials, State Key Laboratory of Silicon Materials, Department of Chemistry, Zhejiang University, Hangzhou 310027, People's Republic of China. E-mail: yizhengjin@zju.edu.cn*
† These authors contributed equally to this work.

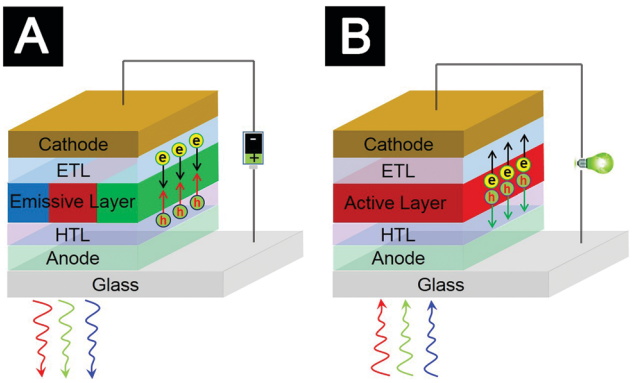

Fig. 1 Typical device structures of solution-processed (A) LEDs and (B) solar cells.

CTLs with desirable properties is critical in terms of improving device performance.

For large-scale production of solution-processed optoelectronics, ideally, not only the active layers but also all the other components should be able to be deposited by solution-based techniques. In this regard, various solution-processed materials have been explored as CTLs. Among them, colloidal metal oxide nanocrystals have attracted great interest.[17–24] The best example is ETLs based on colloidal ZnO nanocrystals, which have been employed in several best-performing proto-type devices, including the quantum-dot LEDs (QLEDs) developed by our group,[18] the quantum-dot solar cells (QDSCs) developed by the Sargent group[22] and the perovskite LEDs developed by the Wang and Huang group.[23] Many other reports showed that colloidal oxide nanocrystals with high work function, *e.g.* NiO nanocrystals,[24,25] can be used to fabricate high-quality HTLs for LEDs and solar cells. Furthermore, colloidal oxide nanocrystals are fully compatible with large-scale industrial production. For example, Krebs and co-workers prepared polymer solar cell modules in which ZnO nanocrystals were deposited as ETLs by a modified slot-die coating procedure.[26,27] These facts highlight a promising future of integrating colloidal oxide nanocrystals as CTLs in solution-processed LEDs and solar cells to achieve high-performance, low-cost and large-area devices.

This review article aims to provide illustrative accounts on the current status of CTLs based on oxide nanocrystals. The progress of utilizing colloidal oxide nanocrystals as CTLs for solution-processed LEDs and solar cells is based on the developments of two important research fields, synthetic chemistry of colloidal oxide nanocrystals and interfacial engineering of optoelectronic devices. There are already good review articles dedicated to either the synthetic chemistry of colloidal oxide nanocrystals[28–32] or interfacial engineering of solution-processed optoelectronics.[33–43] Nevertheless, on the basis of our practices in the past several years, we believe that there is a gap between the community of chemists synthesizing oxide nanocrystals and the community of researchers working on solution-processed optoelectronics. We would like to provide an in-depth review which correlates chemistry of colloidal oxide nanocrystals, processing and optoelectronic properties of CTLs, and device performance of solution-processed solar cells and LEDs. A personal selection of examples is presented to systematize the knowledge bridging the two fields, chemistry of colloidal oxide nanocrystals and interfacial engineering of solution-processed LEDs and solar cells.

Xiaoyong Liang

Xiaoyong Liang is currently a PhD candidate under the supervision of Professor Yizheng Jin in the State Key Laboratory of Silicon Materials, School of Materials Science and Engineering at Zhejiang University. He has keen interest in interfacial engineering of solution-processed optoelectronics using metal oxides as charge-transport layers. Now he is working on quantum dot LEDs.

Sai Bai

Sai Bai obtained his PhD degree in Materials Physics and Chemistry from Zhejiang University in 2014, focusing on solution processable metal oxide films for optoelectronic applications. He is current a VINNMER Fellow and Marie Curie Fellow in Linköping University, Sweden and University of Oxford, UK. His research interests include metal oxide nanocrystals, organic photovoltaics, perovskite solar cells and perovskite light-emitting diodes.

Yizheng Jin

Dr Yizheng Jin is a Professor of Chemistry at Zhejiang University, China. His research interests encompass material chemistry, device engineering and device physics of solution-processed optoelectronics. His research has resulted in over 50 papers in peer-reviewed journals, including Nature, Nat. Photonics, J. Am. Chem. Soc. and Adv. Mater. Prof. Jin has received several awards, including National Natural Science Funds for Excellent Young Scholar, Chinese Chemical Society Award for Outstanding Young Chemist, Qiu-Shi Young Scholars Award and Top 10 scientific advances of 2014 in China.

We will begin with a summary of the general requirements that should be fulfilled by CTLs and point out the unique advantages of colloidal oxide nanocrystals as CTLs. Next, a brief overview of chemistry of colloidal oxide nanocrystals will be presented. Synthetic chemistry of colloidal oxide nanocrystals, ligand chemistry that may be applicable to colloidal oxide nanocrystals and chemistry associated with post-deposition treatments will be covered. The applications of colloidal oxide nanocrystals as CTLs in solar cells and LEDs will be summarized in the subsequent two chapters. Emphasis will be placed on the correlation between the properties of oxide-nanocrystal CTLs and device performance. The last chapter of this review will list three major directions that we believe are critical for future development of oxide-nanocrystal CTLs.

2. General requirements for solution-processed CTLs

An essential requirement for solution-processed CTLs used in optoelectronics is that they should be able to be integrated into devices by solution-based methods. Formulation of inks with sufficiently high concentration and good stability is indispensable to fabricate continuous and pinhole-free CTL films with controllable thickness. For all-solution processed devices, multiple layers, including the ETLs and HTLs, shall be processed from solutions. This often involves the use of orthogonal solvent systems for the deposition of different materials to avoid dissolution of underlying layers. Moreover, processing of top CTLs should exclude high-temperature annealing which may damage the active layers or other components in the devices. Low processing temperatures, *i.e.* <150 °C, are highly desirable so that the processing procedures are compatible with flexible substrates.

CTLs should be of good stability. First and foremost, CTLs themselves must be sufficiently stable within the lifetime of devices. Second, all interfaces involving CTLs, *e.g.* the interfaces of active layer/ETL, active layer/HTL, cathode/ETL and anode/HTL, should be stable and the contact properties should not deteriorate under long-time operational conditions. Third, in device operation, the active layers are in the excited states, which are generally sensitive to oxygen or moisture. The environmental stability of devices can be greatly improved if CTLs act as barriers for oxygen and moisture diffusion.

The chemistry of CTLs should be versatile and robust to allow systematic and purposeful engineering of their optoelectronic properties. Here we use QLEDs and bulk-heterojunction (BHJ) organic solar cells as examples to show that the optoelectronic properties of CTLs, *i.e.* work function, band structure, conductivity, intragap states, optical properties, *etc.*, impact almost all the elementary processes of device operation.

As shown in Fig. 2, elementary processes for QLED operation involve (1) charge injection from electrodes into CTLs, (2) charge transport in the CTLs, (3) charge injection from the CTLs into QD layers, (4) formation of excitons in the QDs, (5) radiative decay of the excitons to generate photons, and

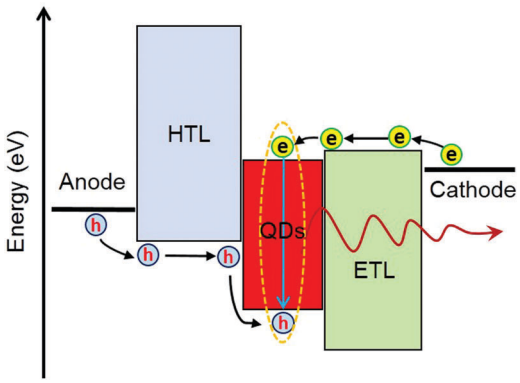

Fig. 2 CTLs and elementary processes for QLED operations.

(6) photon emission out of the devices. The energy-level alignment at the interfaces of electrode/CTLs and QD/CTLs determines the charge injection efficiency. Efficient charge injection into the QDs relies on high conductivity of CTLs and negligible energy barriers at the interfaces to minimize potential-drops. Efficient exciton formation demands both balanced charge injection and effective charge confinement within the QD layer. Charge selective CTLs with good blocking properties are beneficial to realize effective charge confinement. Balanced charge injection requires modulation of both electron injection and hole injection so that injection rates of the two types of carriers can match each other. In general, the ionization potential of many QD emitters is much higher than that of most organic semiconductors. Thus, conventional organic HTLs developed for organic emitters cannot achieve efficient hole injection in QLEDs. Excess injection of one type of charge causes many problems, such as a decrease of the fraction of injected charges that form excitons, charging of QDs which generates less efficient trion emission,[44,45] and deterioration of device lifetime.[18] Interactions between CTLs and excitons formed in QDs often cannot be neglected. This is because the QD films are typically 2–4 monolayers in thickness. Charge recombination zones may locate at regions close to CTLs. CTL-induced quenching can be an important non-radiative decay channel.[46–48] The intragap states of CTLs may act as non-radiative interfacial recombination centers.[46] The last elementary step, *i.e.* escape of the photons out of the devices, largely depends on the optical properties and thickness of the CTLs. Extinction coefficients of the CTLs affect the energy loss of light. Refractive index and thickness of the CTLs are major parameters that modify microcavity effects and energy loss caused by surface plasmon polaritons at the metal electrodes. Based on the above analyses, we conclude that the optoelectronic properties of CTLs impact all the elementary physical processes in QLED operation.

Similarly, the optoelectronic properties of CTLs may influence all the elementary processes of BHJ organic solar cells, in which the active layers consist of blends of electron donors and electron acceptors (Fig. 3). Elementary physical processes in BHJ organic solar cells involve (1) light absorption to generate excitons, (2) exciton diffusion and dissociation at acceptor–donor interfaces to generate charges, (3) charge transport to the corresponding interfaces of active layer/CTLs and (4) charge extraction to external

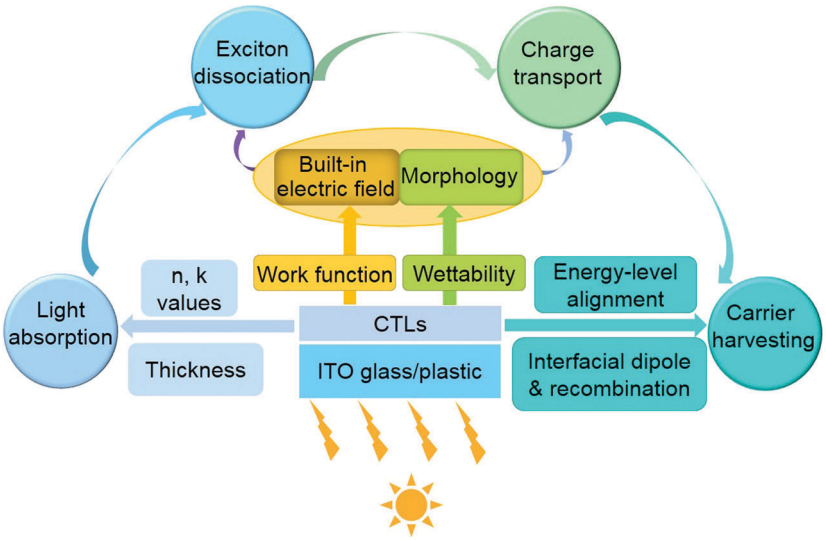

Fig. 3 Impacts of CTLs on the elementary processes of a BHJ organic solar cell.

circuit. Optical properties and thickness of the CTLs can influence distribution of the optical field within a device and energy dissipation in the active layer and thereby affect light absorption.[49] Two important aspects, built-in electric field and morphologies of the BHJ blends, govern the processes of exciton dissociation and charge transport in the active layer.[50] Built-in electric field is largely determined by the work function of the CTLs.[51] Surface-wetting properties of the bottom CTLs may impact film-formation processes of the active layers and hence influence the morphologies of the BHJ blends. At the interfaces of active layer/CTLs, interfacial energy-level alignment and interfacial recombination can tune charge extraction efficiency. And finally, conductivity of the CTLs greatly influences series resistance of the solar cells.

The above analyses suggest that it is crucial to custom-tailor the optoelectronic properties of CTLs to match the active-layer materials and electrodes. Therefore, the chemistry of CTLs should be sufficiently robust to enable on-demand engineering of the material processing and optoelectronic properties.

3. Colloidal oxide nanocrystals and their unique advantages as solution-processed CTLs

Metal oxides are a diverse class of materials which possess very rich optoelectronic properties.[52] Among them, several wide-bandgap semiconductor oxides, including ZnO, TiO_2, SnO_2, NiO, MoO_x, WO_x and VO_x, have been investigated as CTLs for solution processed LEDs or solar cells.[18,37,53–57] They can be classified into three types of materials. ZnO, TiO_2 and SnO_2 are low work-function and n-type oxides, which offer electron transporting and hole blocking properties and thereby can be applied as ETLs. As a p-type wide-bandgap semiconductor with high work function, NiO offers hole transporting and electron blocking properties. MoO_x, WO_x and VO_x are n-type oxides with very deep conduction-band-minimum (CBM) energy levels and high work function. They are another class of widely used HTL materials. But these oxides cannot offer electron blocking properties.[58]

One way to fabricate solution-processed oxide CTLs is to employ colloidal oxide nanocrystals, which are nanometer-sized fragments of the corresponding bulk oxide crystals with surface atoms coordinated by ligands.[4] Surface ligands offer colloidal stability for oxide nanocrystals, enabling them to be processed from solutions to form solid-state films.

An alternative way to fabricate solution-processed oxide CTLs is the so-called precursor approach. In this approach, soluble metal precursors are deposited onto substrates, followed by *in situ* reactions, such as sol–gel hydrolysis[59–61] or combustion reactions,[62] to convert the precursors to oxide films. The precursor approach has also achieved considerable success in the fabrication of oxide films as bottom CTLs for solution-processed optoelectronics.[53,55,60,61,63]

We argue that the nanocrystal approach may offer more freedom than the precursor approach in terms of development of chemistry for solution-processed oxide CTLs and design of the device architecture. A major difference is that the nanocrystal approach decouples crystallization of oxide materials from film-deposition processes, while for the precursor approach, the *in situ* reactions to generate oxides and film-formation processes occur almost simultaneously. In principle, the nanocrystal approach has no restrictions on the syntheses of oxide materials. Harsh reaction conditions, *e.g.* high pressure and high temperature used in the hydrothermal reactions, can be applied to the growth of oxide nanocrystals. Many purification methods, such as extraction or re-crystallization, can be utilized to improve the purity of products. Solubility of oxide nanocrystals can be modulated by ligand-exchange methods.[64,65] Furthermore, deposition of oxide-nanocrystal CTLs can be processed at room temperature.[18,24] In contrast, the precursor approach requires sufficiently high temperature to initiate the *in situ* reactions. Meanwhile, the *in situ* reactions inevitably yield by-products,

such as H_2O. The chemical design of the precursor approach requires the by-products to be volatile so that they can be excluded from the devices. The high temperature and the by-products may cause unwanted side-reactions to other component materials in the devices. These characteristics limit the applications of the precursor approach. As a result, in most solution-processed devices, the precursor approach cannot be applied to fabricate top CTLs. For oxides that require temperatures much higher than 150 °C to convert the precursors to oxides, such as NiO,[66,67] the precursor approach is not compatible with majority of the flexible plastic substrates.

Oxide-nanocrystal CTLs possess distinct electronic and transport properties determined by both the oxide crystals and the surface ligands. From a physics point of view, conduction in oxide-nanocrystal films can be described as hopping of charge carriers between localized electronic states of individual nanocrystals separated by surface ligands. The sizes of ligands or surface-binding motifs determine the shortest possible distances for intra-particle charge hopping. The electronic properties of individual nanocrystals can be influenced by the following factors. Similar to bulk oxide semiconductors, defect chemistry and bandgap engineering such as control over stoichiometry and vacancy and substitutional doping, either isovalent doping or aliovalent doping, can be used to tailor the electronic structure of the oxide crystals. When the sizes of nanocrystals are sufficiently small (comparable to the exciton Bohr radius of the bulk material), quantum confinement effects may take place. Furthermore, surface states induced by chemical bonding between surface atoms and coordinating ligands, vacancies, dangling bonds or adsorbed/weakly bound motifs are extremely important because of the large surface-to-volume ratio. For example, Wang *et al.* demonstrated that charge transport in the ZnO-nanocrystal films is mainly through the surface states by a Mott variable-range hopping process, rather than through the conduction band of the nanocrystals.[68]

Considerable progress has been made in the field of synthetic chemistry of colloidal oxide nanocrystals (see Section 4.1), allowing us to manipulate the electronic properties of individual nanocrystals *via* controlling their composition, size, structure and shape. Despite the excellent colloidal stability and solution processability offered by surface ligands (see Section 4.2), knowledge of ligand chemistry of colloidal oxide nanocrystals is surprisingly scarce. The binding of ligands onto oxide nanocrystals is not fully understood, causing tremendous difficulties in investigating the correlation between surface structures and electronic states. Quantitative information, *e.g.* density and distribution of intragap states and how the energetic disorder of intragap states affects transport properties of the oxide-nanocrystal CTLs, is missing. We highlight that the surfaces of oxide nanocrystals without strong ligand passivation are highly chemically or photo-chemically reactive. Therefore, conduction of the as-prepared oxide-nanocrystal films can be very sensitive to UV irradiation or chemicals in the environments, such as H_2O and O_2. These issues may cause complications for the rational design, processing and applications of oxide-nanocrystal CTLs.

In short, the chemistry of colloidal oxide nanocrystals has advanced substantially in the past few decades, offering excellent low-temperature solution processability which can be tuned by surface chemistry and rich optoelectronic properties which are readily optimized by synthetic chemistry, ligand chemistry and post-deposition chemistry (see Section 4). These two merits, together with the intrinsic stability of oxide materials, which results in enhancement of device lifetime (see Sections 5 and 6), make colloidal oxide nanocrystals a unique class of materials attractive as CTLs for solution-processed LEDs and solar cells.

4. Chemistry related to colloidal metal oxide nanocrystals for CTL applications

4.1 Synthetic chemistry of colloidal oxide nanocrystals

Synthetic chemistry of colloidal oxide nanocrystals allows us to manipulate composition, size, structure and shape of individual nanocrystals, thereby controlling the optoelectronic properties of CTL films, which are assemblies of individual nanocrystals.

Synthetic chemistry of oxide nanocrystals stemmed from the traditional aqueous sol–gel approach, which was used to obtain their bulk counterparts. The traditional aqueous sol–gel approach, however, suffered from high reaction rates, which made it difficult to control the hydrolysis and aggregation processes.[30] In most cases, the traditional aqueous sol–gel approach required an additional high-temperature annealing procedure to induce crystallization. A non-aqueous sol–gel approach was developed to overcome these problems.[29,30,69] In the past two decades, the non-aqueous sol–gel approach has achieved great success. As shown in Scheme 1, reactions based on various molecular mechanisms, including hydrolysis,[24,70–73] alcoholysis,[25,74–81] aminolysis,[78,82–88] and halide elimination,[89,90] were employed to synthesize colloidal oxide nanocrystals. Depending on the reaction pathways, metal precursors and activation reagents with different reactivity and reaction parameters (such as temperature, time and solvent) were carefully selected to control the reaction kinetics and crystallization processes. We list part of the reactions associated with the

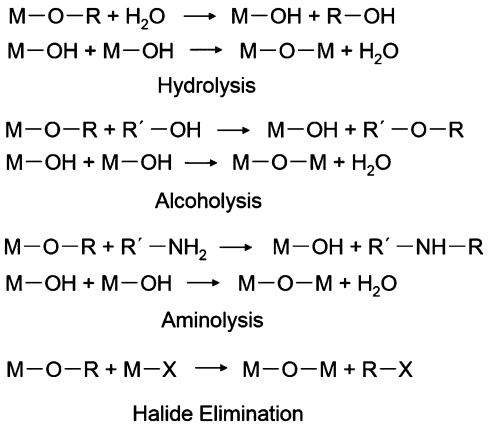

Scheme 1 Reaction pathways associated with the formation of colloidal oxide nanocrystals. M: metal ion, R: alkyl group, X: halide.

formation of oxide nanocrystals for CTL applications in Table 1 and discuss a few important examples in the following sections.

Colloidal ZnO nanocrystals can be synthesized by hydrolysis/condensation reactions conducted under basic conditions. For example, ZnO nanodots were synthesized at room temperature by adding tetramethylammonium hydroxide (TMAH) dissolved in ethanol into a dimethyl sulphoxide (DMSO) solution of zinc acetate ($Zn(Ac)_2$).[72] Similarly, Weller and co-workers demonstrated the synthesis of ZnO nanoparticles at 60 °C by slowly adding KOH into a methanol solution of $Zn(Ac)_2$.[70] An increase in the reaction time led to self-assembly of the ZnO nanodots, which generated nanorods (Fig. 4A and B).[70] Sun *et al.* demonstrated that the molar ratio of zinc precursor to KOH played an important role in determining the stoichiometry of the colloidal ZnO nanostructures and hence affected the conductivity and mobility of oxide films prepared from them.[91]

Colloidal ZnO nanocrystals can also be synthesized *via* alcoholysis or aminolysis. In 2005, Peng and co-workers showed that an ester-formation reaction of zinc stearate and an excess amount of alcohol in 1-octadecene (ODE) at elevated temperatures, *i.e.* >250 °C, generated ZnO nanocrystals with nearly unity yield (Fig. 4C–E).[75] The Niederberger group exploited an aminolysis route to synthesize ZnO nanocrystals.[86] They revealed a reaction mechanism using metal acetylacetonate as one precursor and benzylamine as both an activation agent and a coordination solvent. The alcoholysis and aminolysis can be extended to the syntheses of other oxide nanocrystals. For example, Murray and co-workers synthesized TiO_2 nanocrystals with different shapes by alcoholysis or aminolysis reactions of halotitanium carboxylate complexes.[83]

Halide elimination reaction was first applied to the synthesis of colloidal TiO_2 nanocrystals by Colvin *et al.* in 1999.[90] The reaction of titanium halide and titanium alkoxide in the presence of trioctylphosphine oxide (TOPO), which functioned as a stabilizer to ensure good dispersion of the resulting nanocrystals in nonpolar solvents, led to TiO_2 nanocrystals with pure anatase phase. This reaction was further extended to realize shape control of TiO_2 nanocrystals by Alivisatos and co-workers.[89] They found that TiO_2 nanocrystals with shapes ranging from bullet, rod to branched-rod could be obtained by adjusting the amounts of lauric acid and TOPO in the reaction mixture.

Hydrothermal or solvothermal synthesis provides an additional dimension to modulate reactivity of precursors and crystallization of oxides. Niederberger and co-workers conducted a series of reactions between metal halides (or metal acetylacetonates) and benzyl alcohol (or benzylamines, ketones, acetonitrile), which resulted in many colloidal oxide nanocrystals, including TiO_2, ZnO, In_2O_3, and WO_x.[69,74,86,92–98] Wang *et al.* have successfully exploited a hydrothermal method to synthesize highly crystalline SnO_2 nanocrystals.[73] Further manipulation of the reaction conditions can provide shape-controlled oxide nanocrystals,

Table 1 Syntheses of colloidal oxide nanocrystals applicable as CTLs. Abbreviations: $Zn(St)_2$, zinc stearate; ODA, 1-octadecanol; ODE, 1-octadecene; $Zn(Ac)_2$, zinc acetate; TMAH, tetramethylammonium hydroxide pentahydrate; OAc, oleic acid; OAm, oleyl amine; $Ti(OPr^i)_4$, titanium tetraisopropoxide; $Ti(OR)_4$ [R = alkyl group]; $Ni(acac)_2$, nickel(II) acetylacetonate; DMSO, dimethyl sulphoxide

Oxide	Reagents	Conditions	Molecular mechanism	Ref.
ZnO	$Zn(St)_2$, ODA	ODE; 250 °C	Alcoholysis	75
ZnO	$Zn(acac)_2{\cdot}xH_2O$	Benzylamine; 200 °C; 2 days	Aminolysis Solvothermal	86
ZnO	$Zn(acac)_2{\cdot}xH_2O$	Benzyl alcohol; 120 °C; 24 h	Alcoholysis	79
ZnO	$Zn(Ac)_2$, TMAH	DMSO; 30 °C	Hydrolysis	72
ZnO	$Zn(Ac)_2$, KOH	Methanol; 60 °C; 2 h	Hydrolysis	70
TiO_2	$Ti(OPr^i)_4$, H_2O	OAc; 80 °C	Hydrolysis	71
TiO_2	$Ti(OC_4H_9)_4$, OAc, OAm	OAc; 180 °C; 18 h	Alcoholysis Aminolysis	78
TiO_2	$Ti(OPr^i)_4$, OAm	Benzyl alcohol; 180 °C; 24 h	Alcoholysis Solvothermal	77
TiO_2	TiX_4, $Ti(OR)_4$	Heptadecane; 300 °C; 5 min	Halide Elimination	90
TiO_2	$TiCl_4$, $Ti(OPr^i)_4$	Dioctyl ether; 300 °C;	Halide Elimination	89
TiO_2	$TiCl_4$	Benzyl alcohol; 40 °C	Alcoholysis	74
TiO_2	$TiCl_4$, TiF_4, OAc, OAm	ODE; 290 °C	Aminolysis	83
NiO	$Ni(NO_3)_2{\cdot}6H_2O$	Octadecylamine; 180 °C; 10 min	Aminolysis	87
NiO	$Ni(St)_2$, LiSt, ODA	ODE; 235 °C; 3 h	Alcoholysis	25
NiO	$Ni(acac)_2$	*tert*-Butanol; 200 °C	Alcoholysis Solvothermal	81
WO_x	$W(CO)_6$, OAm	OAm; 270 °C; 2 h	Aminolysis	84
WO_x	$W(OC_2H_5)_5$, TOA	OAc; 350 °C; 5 min	Aminolysis	88
WO_x	WCl_6, deferoxamine mesylate (DFOM)	Benzyl alcohol; 100–175 °C; 48 h	Alcoholysis Solvothermal	76
WO_x	WCl_6	Ethanol; 180 °C; 24 h	Alcoholysis Solvothermal	80
SnO_2	$SnCl_4{\cdot}5H_2O$, TMAH	Ethanol; 100 °C; 12 h	Hydrolysis Hydrothermal	73
V_2O_3	$VO(acac)_2$, OAc, OAm	Squalane; 310–370 °C; 1 h	Aminolysis	82
VO_2	$VOCl_3$, OAm	OAm; 250 °C; 20 min	Aminolysis	85

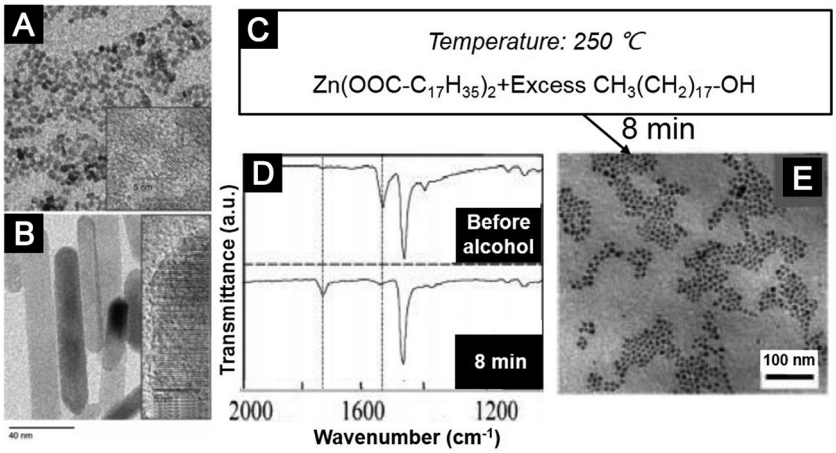

Fig. 4 (A and B) Colloidal ZnO nanocrystals synthesized by the hydrolysis approach. Typical TEM images of (A) ZnO nanodots and (B) ZnO nanorods (grown by the self-assembly of nanodots). (C–E) Colloidal ZnO nanocrystals synthesized by the alcoholysis approach. (C) Reagents and reaction conditions. (D) FTIR spectra to reveal the molecular mechanism. (E) A typical TEM image of the ZnO nanocrystals. (A and B) Reprinted with permission from ref. 70. Copyright 2002 Wiley-VCH. (C–E) Adapted with permission from ref. 75. Copyright 2005 American Chemical Society.

such as colloidal TiO_2 nanosheets and rhombic TiO_2 nanocrystals with exposed high-energy facets.[77]

Identifying molecular pathways and quantifying chemical kinetics can provide valuable information to understand the chemical reactions associated with the formation of oxide nanocrystals. This can be done by tracing the organic by-products. For example, by-products of alcoholysis and hydrolysis reactions of metal carboxylates are ester and acid, respectively, which show distinctly different absorption features in the Fourier transform infrared spectroscopy (FTIR).[99,100] We carried out a series of temperature-dependent FTIR measurements on a variety of metal carboxylates.[100,101] The results inspired us to control reaction pathways by modifying experimental procedures and selecting metal precursors with adequate reactivity. Furthermore, we developed an experimental method based on FTIR to measure the initial reaction rates of the alcoholysis reactions of metal carboxylates (Fig. 5).[102] This method allowed us to quantitatively compare reactivity of different metal precursors under given reaction conditions and obtain important kinetic parameters, such as activation energy. In another report, Niederberger and co-workers investigated the molecular mechanism and crystallization of ZnO nanocrystals synthesized by the benzyl alcohol route.[79] They used gas chromatography to quantify the organic by-products and concluded that the rate-limiting step for the formation of ZnO nanocrystals was the generation of the monomer species.

Mechanistic understanding at the molecular level is beneficial for rational design of synthetic chemistry of colloidal oxide nanocrystals. For example, we identified that the synthesis of pure colloidal NiO nanocrystals by alcoholysis of metal carboxylates was plagued by an unwanted side reaction, *in situ* reduction of NiO nanocrystals by alcohol at elevated temperatures.[25] In this regard, we introduced lithium stearate, an ionic molecule which is stable in the reaction system and capable of binding onto the surface of NiO nanocrystals to suppress their reactivity. This ligand-protection strategy (Fig. 6) prevented the reduction reactions, leading to pure and high-quality NiO nanocrystals with a high yield.

Knowledge of molecular mechanisms and reaction kinetics is critical for controlled doping of oxide nanocrystals. Introduction of specific dopants is a general approach to modify the properties of nanocrystals in well-controlled ways. Isovalent doping, *i.e.* alloying, can modulate the bandgap energy of nanocrystals.[72,99] Our group demonstrated the syntheses of Mg-doped ZnO nanocrystals and Cd-doped ZnO nanocrystals with tuneable optical bandgaps ranging from 3.3 to 3.9 eV (Fig. 7A).[99,101] We discovered interesting dopant induced shape evolution for these doped oxide nanocrystals, which was later observed in many other doped colloidal nanocrystal systems.[103–105] Aliovalent doping can generate additional free carriers in oxide nanocrystals,[100,106–113] which may lead to enhanced conductivity and modified work function of the films processed from the doped oxide nanocrystals (Fig. 7B and C). Typical examples are ZnO nanocrystals doped with group III elements of Al^{3+}, Ga^{3+} or In^{3+},[106–112] and TiO_2 nanocrystals doped with Nb^{5+}.[114,115] At the molecular level, successful doping of oxide nanocrystals is likely to be a result of *in situ* incorporation of the dopant ions during the growth of the host oxide nanocrystals. A key issue linking chemical reactions and crystallization processes of doped oxide nanocrystals is that adequate host crystal growth and dopant incorporation rates rely on balanced host–dopant precursor reactivity.[116] Milliron and co-workers found that for the synthesis of Al-doped ZnO nanocrystals, successful doping was achieved when zinc stearate and aluminium acetylacetonate were selected as precursors.[106] No doping was observed when the dopant precursor was replaced by the less reactive aluminium stearate. Our group employed the synthesis of Mg-doped ZnO nanocrystals as a model system to quantitatively study the correlation between chemical kinetics of the precursor conversion reactions and formation of doped nanocrystals under synthetic conditions.[102] The results showed that three independent factors, molar ratio of the dopant precursor, reaction temperature and coordination ligands of cationic precursors, influenced the relative reactivity

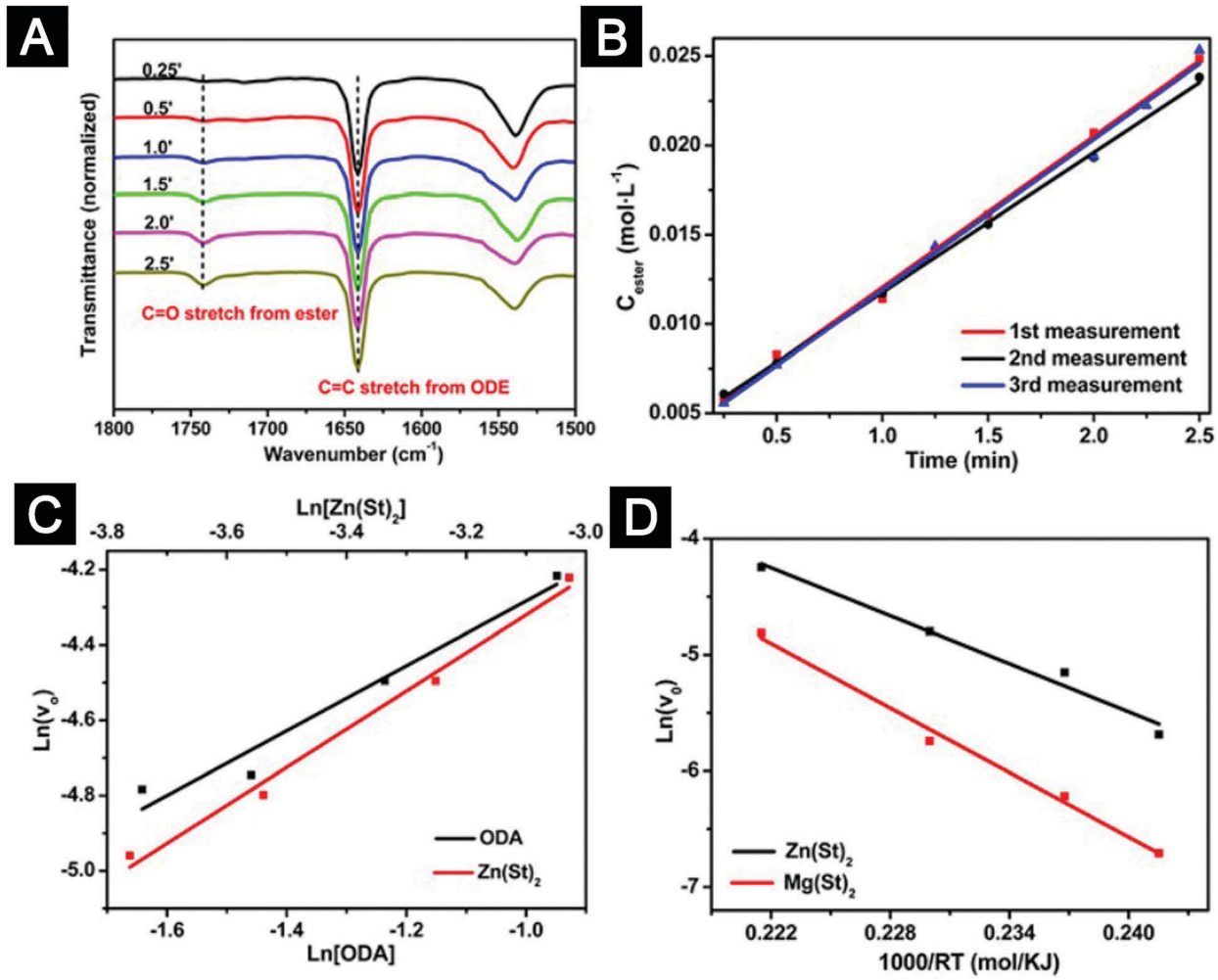

Fig. 5 A quantitative method based on FTIR to study the chemical kinetics of the alcoholysis reactions of metal carboxylates. (A) Temporal evolution of FTIR spectra recorded from an alcoholysis reaction. (B) Determination of the initial reaction rates. (C) Determination of the reaction orders for $Zn(St)_2$ and ODA from the plot of the initial formation rate of ester *versus* the concentration of $Zn(St)_2$ and the plot of the initial formation rate of ester *versus* the concentration of ODA, respectively. (D) Irving plots of the initial reaction rates of alcoholysis reactions. Abbreviations: ODE, 1-octadecene; ODA, 1-octadecanol; $Zn(St)_2$, zinc stearate; $Mg(St)_2$, magnesium stearate. Figures reprinted with permission from ref. 102. Copyright 2014 Macmillan Publishers Limited.

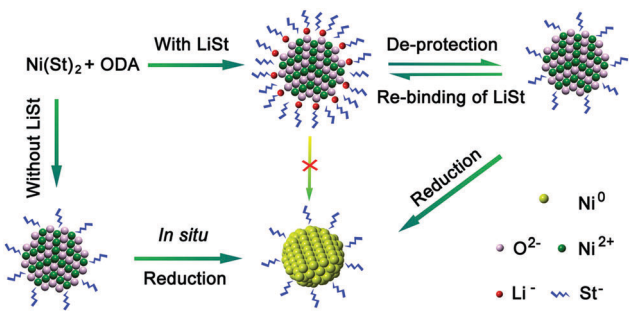

Fig. 6 Synthesis of colloidal NiO nanocrystals with LiSt as the protecting ligand. Abbreviations: ODA, 1-octadecanol; LiSt, lithium stearate; $Ni(St)_2$, nickel stearate. Figure reprinted with permission from ref. 25. Copyright 2014 American Chemical Society.

of magnesium to zinc precursor and thereby the syntheses of Mg-doped ZnO nanocrystals with different shapes and properties.

Balancing the reactivity of the dopant to host precursors can be a decisive factor which ensures successful incorporation of dopants into host lattices, avoiding unwanted phase segregation of host-oxide crystals or dopant-oxide crystals.

4.2 Ligand chemistry related to colloidal oxide nanocrystals

Surface ligands provide essential colloidal stability and processability for oxide nanocrystals. Surface ligands play multiple roles in influencing the optoelectronic properties of CTLs based on oxide nanocrystals. The bonding of surface ligands passivates dangling bonds, which modulates the intragap states of the oxide materials. In most cases, the sizes of ligand molecules determine the shortest charge hopping distances and therefore affect charge transport processes in assemblies of oxide nanocrystals. Furthermore, ligand-induced surface dipoles can shift the absolute energy levels of nanocrystal films.[117]

The importance of surface ligands can hardly be overemphasized. Nevertheless, a quantitative description of binding

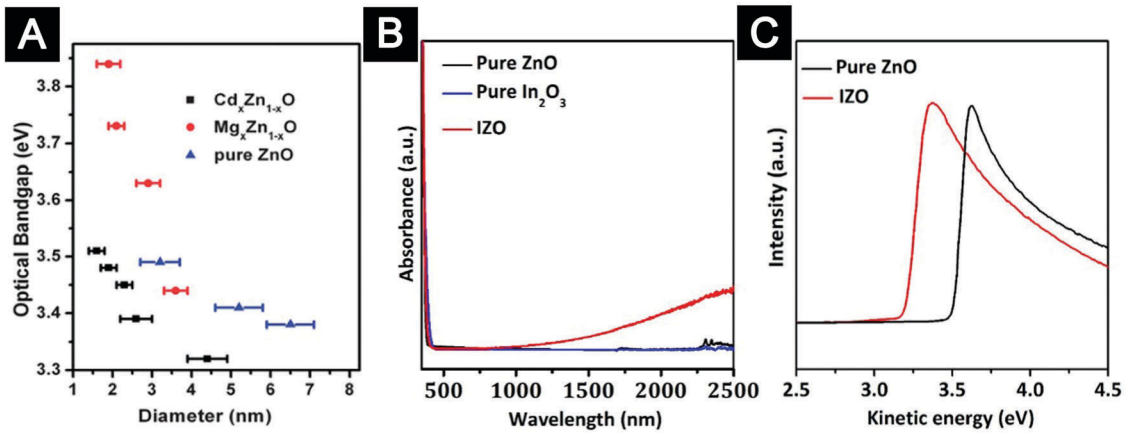

Fig. 7 Doping chemistry to control the properties of colloidal ZnO nanocrystals. (A) Optical bandgaps of the pure ZnO, alloyed $Cd_xZn_{1-x}O$, and $Mg_xZn_{1-x}O$ nanocrystals with different sizes. (B) Normalized UV-Vis-NIR spectra of indium doped ZnO (IZO) nanocrystals, ZnO nanocrystals and In_2O_3 nanocrystals. The surface plasmon resonance peak in the near-infrared region indicated high density of free electrons in the IZO nanocrystals. (C) Secondary electron cut-off edge of UPS spectra showing that indium doping resulted in a lower work function of the oxide-nanocrystal films. (A) Reprinted with permission from ref. 101. Copyright 2013 Royal Society of Chemistry. (B and C) Reprinted with permission from ref. 100. Copyright 2014 American Chemical Society.

of ligands onto oxide-nanocrystal surfaces is still lacking. This situation causes tremendous difficulties in investigating the correlation between surface structures and surface electronic states. We shall present some recent progress of ligand chemistry in the nanocrystal field, which is not limited to the oxide nanocrystal field. We believe that understanding from these examples may shed light on the rational design of ligand chemistry of oxide nanocrystals for CTL applications.

The covalent bond classification (CBC), an established concept in coordination chemistry, provides a general framework to describe the binding of surface ligands and to rationalize ligand exchange and displacement reactions (Fig. 8A–C).[118–120] The CBC treats bonding as a 2-center-2-electron interaction. Ligands can be classified as L- X-, or Z-type, depending on the number of electrons contributed to the bonding orbitals from the neutral ligands (2, 1, or 0, respectively). L-type ligands, such as R-NH_2 and P-R_3, are neutral donors that are datively bound to surface metal atoms. Z-type ligands, such as carboxylate salts, are neutral accepters that are datively bound to surface non-metal atoms. X-type ligands are bound to either metal or non-metal atoms, depending on their affinity.[119] Owen and co-workers used FTIR and nuclear magnetic resonance (NMR) to study ligand exchange and ligand displacement reactions of metal–chalcogenide nanocrystals, *e.g.* CdSe, CdS and PbS nanocrystals.[120] They demonstrated that the surface reactions between Z-type ligands and L-type ligands could be well-justified within the framework of CBC (see Fig. 8C for details). The Hens group employed HfO_2 nanocrystals as a model system for oxide nanocrystals and carried out a series of investigations on the surface bonding and ligand-exchange reactions.[121–123] Their results showed that the as-synthesized HfO_2 nanocrystals, which were charge-stabilized by protons with chloride as counter ions, were transferred to non-polar solvents by using a mixture of carboxylic acids and amines. The key finding was that, in contrast to CdSe nanocrystals, the surface of oxide nanocrystals absorbed protons. Both the carboxylate, an anionic X-type ligand, and the proton, a cationic X-type ligand, bound to the surface of HfO_2 nanocrystals, which was denoted as X_2-type binding. They further demonstrated reversible and chemical-driven ligand displacement reactions between the surface-bound carboxylic acid and amines or alcohols in solution (see Fig. 8D). Ligand exchange using X-type ligands, such as silanes and phosphonates, was also reported.[124–126] We expect that these findings can be applied to understand the surface bonding features and surface chemical reactions of oxide nanocrystals for CTL applications.

Another critical issue is that surface ligands need to fulfil demands from the aspects of both solution processability and charge transport. In conventional models, steric separation between nanocrystals by surface ligands improves the colloidal stability of the nanocrystal solutions. Therefore, ligands with long hydrocarbon chains, *e.g.* oleic acid or oleyl amine, were used in many non-aqueous sol–gel syntheses. However, these insulting ligands, acting as energy barriers for charge transport, are not suitable for CTL applications.

In the nanocrystal field, a number of ligand-exchange strategies have been proposed, including ligand exchange with smaller molecules, thermal-degradable ligands or metal–chalcogenide complexes (MCCs), to solve this problem.[65,127–130] Nevertheless, these existing ligand-exchange strategies may be of limited value for oxide nanocrystals towards CTL applications. Short ligands may cause poor stability of colloidal solutions. Thermal-degradable ligands, which are produced by sophisticated molecular design and synthetic procedures, need additional thermal annealing to initiate decomposition reactions and generate gaseous by-products.[129,130] Therefore these thermal-degradable ligands cannot be applied to the fabrication of top CTLs. The MCC ligands have achieved success in fabricating highly conductive films based on metal nanocrystals and high-mobility films based on semiconductor nanocrystals.[127,131] Nevertheless, the MCC ligand-capped nanocrystals are stable

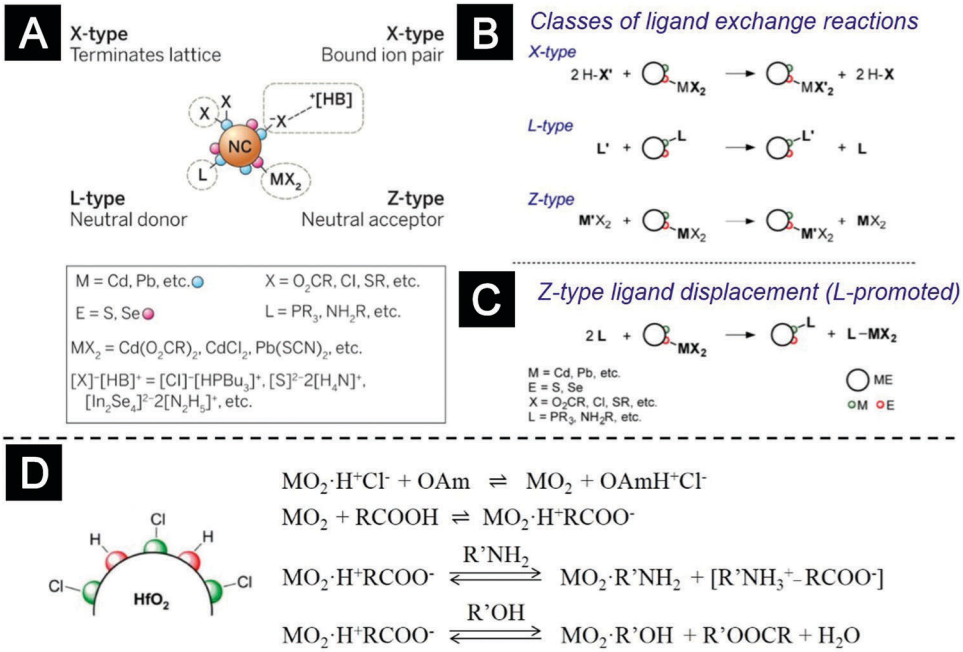

Fig. 8 Ligand chemistry of nanocrystals. (A) Schematic representation of the covalent bond classification (CBC) to describe ligand–nanocrystal binding. (B and C) Examples of surface-modification reactions of metal chalcogenide nanocrystals, including (B) X-, L-, and Z-type exchange and (C) Z-type ligand displacement. (D) Surface bonding and ligand-exchange reactions of HfO_2 nanocrystals. R: alkyl group, Bu: *n*-butyl, M: metal ion, OAm: oleyl amine. (A) Reprinted with permission from ref. 119. Copyright 2015 American Association for the Advancement of Science. (B and C) Reprinted with permission from ref. 120. Copyright 2013 American Chemical Society. (D) Adapted with permission from ref. 123. Copyright 2014 American Chemical Society.

only in polar solvents with a very high dielectric constant like dimethylformamide. Such solvents have considerable drawbacks, such as toxicity and high boiling point. In addition, the use of MCC ligands for oxide nanocrystals shall generate thin films of oxide–metal chalcogenide complexes, which may create high density of electronic states within the bandgap of the oxides.

In 2016, the Peng group introduced the concept of ''entropic ligands''. They used CdSe nanocrystals coated with stearate ligands as a model system and discovered strong size- and temperature-dependent solubility of CdSe nanocrystals in organic solvents.[132,133] The experimental results can be quantitatively explained by a thermodynamic model based on the precipitation/dissolution phase transition (see Fig. 9A). By making reasonable approximations, the molar faction of the nanocrystal–ligand complexes, χ, can be expressed by a simple equation,

$$\chi = e^{-\Delta^m H_{NC}/RT} e^{\Delta^m S_{NC}/R}$$

where $\Delta^m H_{NC}$ is the partial molar mixing entropy of the nanocrystal–ligand complexes dissolving in a liquid and $\Delta^m S_{NC}$ is the molar conformational entropy, which accounts for the melting entropy of the complex solid. The analyses revealed that the conformational entropy of the *n*-alkanoate chain released in solution, *i.e.* the rotational and bending entropy related to the C–C sigma-bonds, exponentially increases the solubility of the nanocrystal–ligand complexes while the strong chain–chain interactions between adjacent particles in solids decrease the solubility. This finding inspired the authors to introduce 'entropic ligands' with irregularly branched alkyl chains, which maximize intramolecular entropy and minimize enthalpy for destructing the crystalline chain–chain interactions (Fig. 9B). The use of entropic ligands boosted the solubility of CdSe nanocrystals to several hundreds of mg mL^{-1}, which was increased by $\sim 10^3$ to 10^5 compared to that of the nanocrystals with *n*-alkanoate ligands. The concept of entropic ligands was proven to be effective for a number of other nanocrystals, including Fe_3O_4 nanocrystals, and a variety of organic solvents (Fig. 9C). It is therefore possible to simultaneously improve processability of colloidal nanocrystals in solution and charge transport of their corresponding films (Fig. 9D). For example, electrical measurements on the electron-only devices showed that the conductivity of films based on CdSe nanocrystals coated with 2-ethyl-hecanethialate ligands increased by $\sim 10^3$ in comparison with that of films based on CdSe nanocrystals coated with octadecanethiolate ligands. We fabricated QLEDs using CdSe/CdS core/shell QDs with different ligands. The results showed that the use of 2-ethyl-hecanethialate as surface ligands improved the external power efficiency (EPE) of the QLEDs by $\sim$30% due to the improved charge transport of the QD films. These exciting results suggested that the concept of entropic ligands should be an important guideline for future design of surface ligands of colloidal oxide nanocrystals.

4.3 Chemistry of post-deposition treatments of oxide-nanocrystal films

The properties of oxide-nanocrystal films, including conductivity, work function, intragap states, and surface-wetting properties, can also be modified by post-deposition treatments, partially

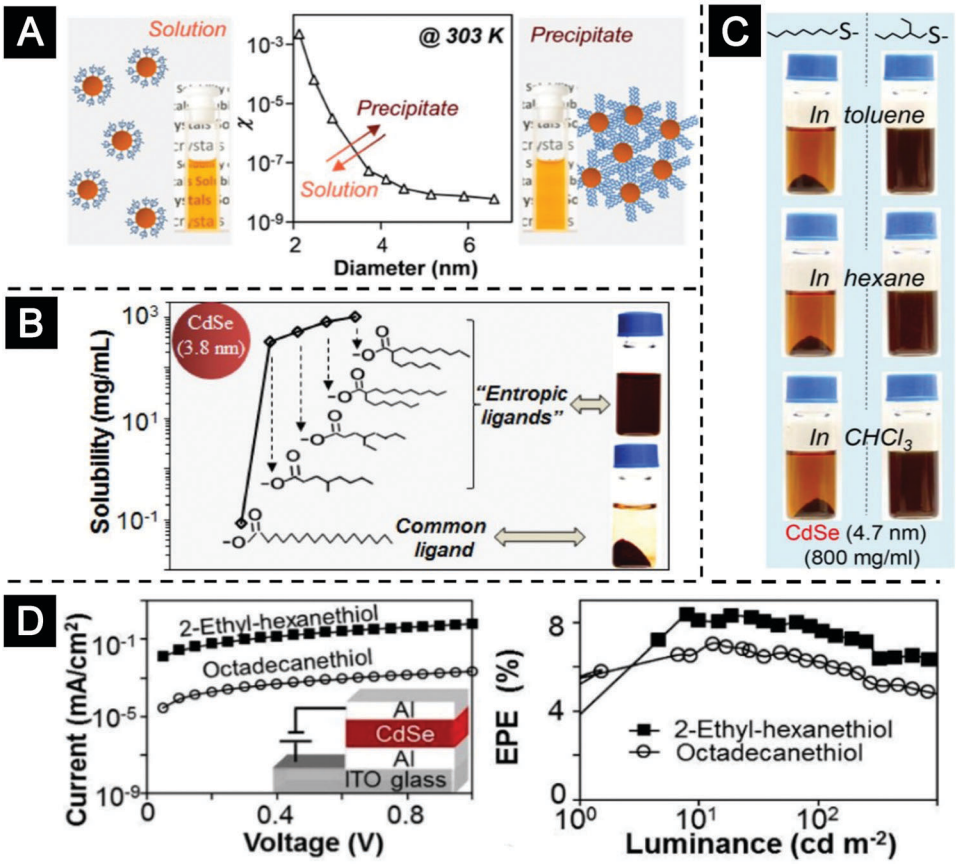

Fig. 9 Entropic ligands for nanocrystals. (A) Schematic representation and solubility data of the thermodynamic model based on the precipitation/dissolution phase transition. (B) The use of entropic ligands increased the solubility of CdSe nanocrystals by 3–4 orders of magnitude. (C) Digital photos of CdSe nanocrystals with stearate (left column) or 2-hexyl-ecanoate (right column) as ligands in four solvents at 303 K. (D) The use of entropic ligands improved the charge transport of the QD films. Figures reprinted with permission from ref. 132 and 133. Copyright 2016 American Chemical Society.

attributed to the chemically active large surface areas of the oxide nanocrystals. We briefly discuss the chemistry of several widely used post-deposition treatments. More details of post-deposition treatments related to a specific device will be covered in Sections 5 and 6. We note that most post-deposition treatments can only be applied to bottom CTLs, but not top CTLs since post-deposition treatments may deteriorate the properties of other materials in the devices as well.

Thermal annealing at elevated temperature can efficiently remove residual solvent molecules. Ligands with relatively weak binding affinity to the oxide surfaces may be dissociated from surfaces, causing sintering or necking of the oxide nanocrystals.[100] Depending on the annealing temperature and atmosphere, different chemical reactions may take place and cause significant changes in the film properties.[24] Surface ligands may react with water if the oxide-nanocrystal films were annealed under ambient conditions, which may modify the intragap states.[134] Annealing oxide-nanocrystal films in a reductive (or oxidative) atmosphere can increase (or decrease) the density of oxygen vacancy, leading to significant changes in electronic properties. For example, it was shown that the electron mobility and sheet resistance of ZnO-nanocrystal films could be tuned by over three orders of magnitude *via* controlling the annealing conditions from an oxidative atmosphere to a reductive one.[135]

UV-ozone treatment and oxygen-plasma treatment are two violent methods to change the optoelectronic properties of oxide-nanocrystal films. We use UV-ozone treatment of NiO-nanocrystal films as an example to illustrate the multiple reactions that may take place.[25] UV-ozone treatment can remove organic ligands due to the strong oxidation activity, leading to sintering or necking of oxide nanocrystals which increases the conductivity of the NiO-nanocrystal thin films.[25] It has been demonstrated that the UV-ozone treatment also changed the valence states and stoichiometry of surface ions.[136] X-ray photoelectron spectroscopy investigations further revealed that UV-ozone treatment created surface species of nickel oxyhydroxide (NiOOH). The dipolar species are responsible for the increase of work function from ~4.8 eV to ~5.1 eV after UV-ozone treatment. Similarly, Zhang *et al.* reported that the work function of NiO-nanocrystal thin films can be increased from ~4.8 eV to ~5.3 eV by O_2-plasma treatment.[137]

The interfacial properties of oxide-nanocrystal films can be modified by introducing additional molecules or layers, either by chemical covalent bonding or by physical adsorption.

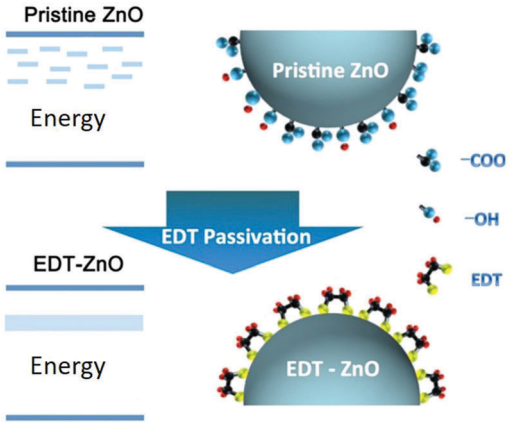

Fig. 10 Modulation of the intragap states of the ZnO-nanocrystal films by EDT treatment. Figure adapted with permission from ref. 19. Copyright 2014 Wiley-VCH.

Polyethylenimine ethoxylated (PEIE) or branched polyethylenimine (PEI) are polymers containing simple aliphatic amine groups. Physisorption of an ultrathin layer of these polymers onto the surfaces of oxide-nanocrystal films induced interfacial dipoles, which reduced the work function of the oxide-nanocrystal films, as revealed by ultraviolet photoemission spectroscopy (UPS) and Kelvin probe measurements.[138] The modification of surface work function can also be realized by using covalently bonded self-assembled monolayers (SAMs). For example, the work function of ZnO films can be controlled by a SAM of molecules derived from benzoic acid derivatives with different dipole orientations.[139] The covalent bonding of additional molecules onto the surfaces of oxide nanocrystals can efficiently modulate the intragap states of the films. We developed a simple passivation method based on ethanedithiol (EDT) treatment for ZnO-nanocrystal films (Fig. 10).[19] The surface defects of the ZnO-nanocrystal films including surface groups, such as hydroxyl groups and carboxylate groups, and dangling bonds were removed by forming zinc ethanedithiolates, which introduced a new intragap band.

5. Recent developments of CTLs based on colloidal oxide nanocrystals for solution-processed LEDs

5.1 Solution-processed organic LEDs (OLEDs)

Electroluminescence from conjugated polymers was first demonstrated in 1990, using poly(*p*-phenylene vinylene) (PPV) as a single semiconductor layer sandwiched between metallic electrodes.[1] Since then, solution-processed OLEDs have experienced significant advances in the past ~25 years. Intensive work on synthetic chemistry, together with new understanding on photo-physics, has now led to many solution-processed organic materials with good emissive properties, including polymers, dendrimers and small molecules.[140–144] Innovations on device architectures and the corresponding CTLs were made to optimize charge balance and achieve long operational lifetime.

In the early stages, poor electron injection was one of the limiting factors for solution-processed OLEDs due to the relatively high energy offset between the lowest-unoccupied-molecular-orbital (LUMO) energy levels of organic emitters and the Fermi levels of electrodes. Metals with low work function, such as Ca or Ba, were used to facilitate electron injection into organic layers. However, these low-work-function metals and the interfaces of polymer/metal are unstable, resulting in poor device stability. Furthermore, the most widely used hole injection material, poly(3,4-ethylenedioxythiophene)-poly(styrene sulfonate) (PEDOT:PSS), suffers from hygroscopicity and acidic nature. These facts inspired scientists to introduce solution-processed oxides as CTLs for organic LEDs.[141,145] Here we focus on the applications of colloidal oxide nanocrystals as CTLs in solution-processed OLEDs.

Haque and co-workers introduced nanocrystalline TiO_2 thin films as ETLs for polymer LEDs in 2007.[146] Although the efficiency of this device was modest, the device performance was enhanced compared with the devices without TiO_2 ETLs. Qian *et al.* applied ZnO-nanocrystal ETLs in polymer LEDs with poly[2-methoxy-5-(2-ethylhexyloxy)-1,phenylene vinylene] (MEH-PPV) emitters.[147] Sessolo *et al.* employed ZnO nanocrystals as ETLs in flexible polymer LEDs on plastic substrates, leading to very bright poly(9,9-dioctylfluorene-*alt*-benzothiadiazole) (F8BT) electroluminescence.[148] The turn-on voltages of the devices using ZnO-nanocrystal ETLs are lower than the corresponding energy gaps of the luminescent materials, indicating efficient electron injection. The Auger assisted energy up-conversion process occurring at the polymer/ZnO nanocrystal interface was invoked to explain this sub-bandgap turn-on phenomenon.[147] This mechanism is plausible. Sub-bandgap turn-on at room temperature was commonly observed for the vacuum-deposited high-efficiency inorganic LEDs with ohmic contacts.[149]

The performance of solution-processed OLEDs can be optimized by tuning the properties of oxide-nanocrystal ETLs. Here we selected a few examples of LEDs using F8BT as an emissive material and ZnO nanocrystals as ETLs to highlight the importance of controlling the interface of emissive organics/oxide nanocrystals.[100,150,151] In general, an energy barrier for electron injection exists at the ZnO/F8BT interface. This electron injection barrier can be modulated by adjusting the work function of the ZnO ETLs. Our group synthesized indium-doped ZnO (IZO) nanocrystals with high density of free carriers. The indium doping accompanied by filling free electrons into the conduction band generated an up-shift of ~0.3 eV in the Fermi level of the oxide ETLs (Fig. 11A).[100] Scanning Kelvin probe microscopy (SKPM) results on the bilayers of F8BT/IZO nanocrystal thin films showed that the surface potential of the IZO-nanocrystal layer was more positive than that of the F8BT layer, while in the case of the F8BT/ZnO nanocrystal bilayer, the surface potential of the ZnO-nanocrystal layer was more negative than that of the F8BT layer (Fig. 11B and C). Therefore, the IZO-nanocrystal ETLs offered improved efficient injection properties. As a result, the PLEDs based on IZO ETLs exhibited much better performance, *i.e.* lower turn-on voltages, higher maximum luminance and higher efficiency, compared with the devices

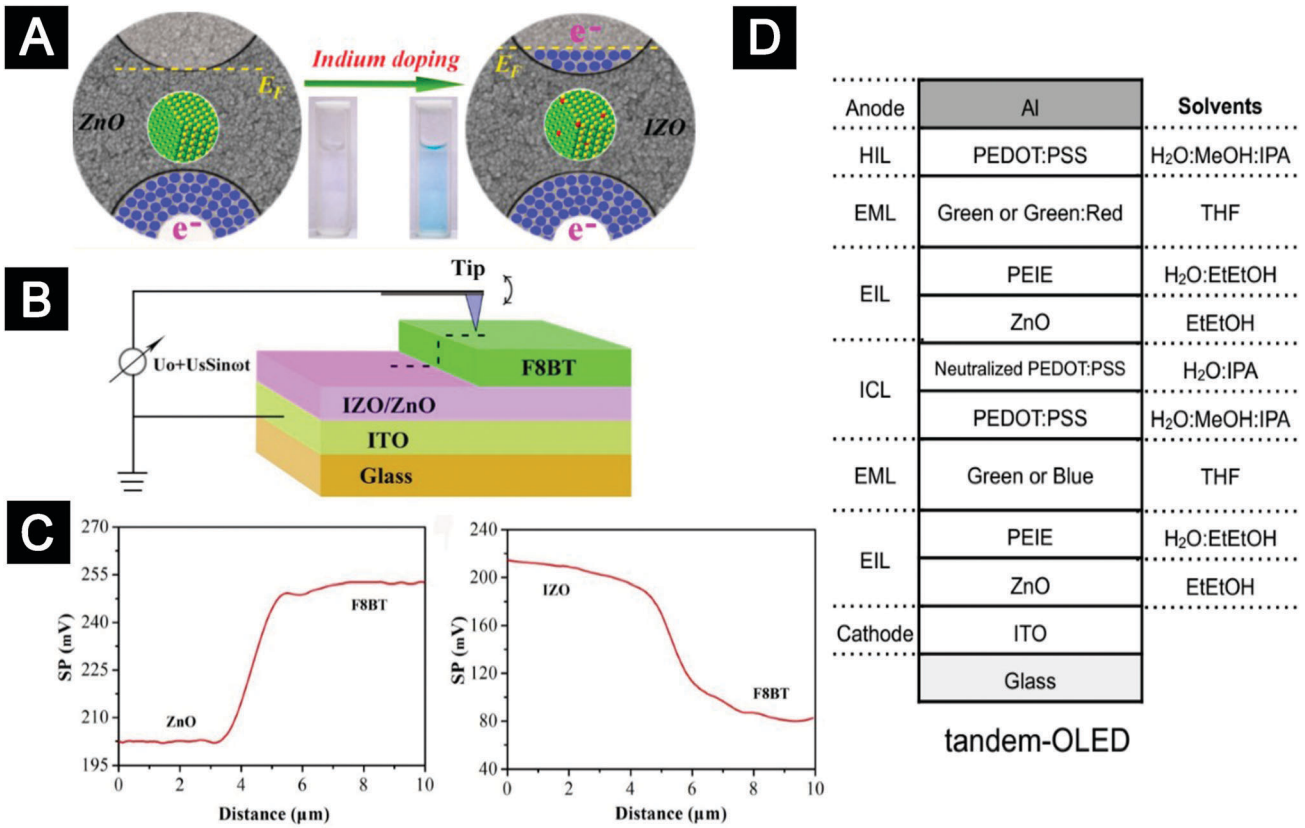

Fig. 11 (A–C) IZO nanocrystals as ETLs for solution-processed OLEDs. (A) Indium doping led to a population of free electrons in the conduction band of ZnO nanocrystals, which lowered the work function of the oxide-nanocrystal films. (B) Schematic illustration of the SKPM measurement setup for bilayers of oxide films/F8BT. (C) Surface potential line-profiles crossing the height-step of the bilayers of ZnO/F8BT (left) and IZO/F8BT (right). (D) Tandem OLEDs with ICL composed of ZnO nanocrystals/PEIE and PEDOT:PSS. (A–C) Reprinted with permission from ref. 100. Copyright 2014 American Chemical Society. (D) Reprinted with permission from ref. 151. 2015 Wiley-VCH.

based on ZnO ETLs. The Kido group found that the electron injection efficiency at the ZnO/F8BT interface could be improved by using lithium quinolate complex (Liq) or $CsCO_3$-doped ZnO nanocrystals.[150] The same group also investigated the performance of size- and shape-controlled ZnO nanoparticles as ETLs in OLEDs.[151] Introducing an interfacial dipole layer is another important strategy to lower the work function of the ZnO-nanocrystal ETLs. For example, indium-tin-oxide (ITO) free and all-solution-processed transparent OLEDs with PEI modified ZnO nanocrystal thin films as ETLs were reported by Zhang and co-workers.[152] Remarkably, the ZnO/PEI bilayer can tolerate many solvents used for the subsequent deposition of top layers, making it applicable as a charge generation layer in tandem structured OLEDs. Recently, solution-processed tandem OLEDs with the interconnecting layer comprised of PEI modified ZnO and WO_3 were realized by Höfle and co-workers.[153] Later, Kido and co-workers reported solution-processed phosphorescent tandem OLEDs with improved performance by combining ZnO nanocrystals/PEIE and PEDOT:PSS as an interconnecting conductive layer (Fig. 11D).[151,154] The resulting tandem-OLED exhibited impressive efficiencies, reaching 26% and 28% of external quantum efficiency (EQE) at 5000 cd m^{-2} for green and white OLEDs, respectively.

Apart from ZnO and TiO_2, other n-type oxide nanocrystals have also been applied as ETLs in solution-processed OLEDs. For example, Lee *et al.* introduced SnO_2 nanoparticles as ETLs to fabricate phosphorescent OLEDs due to their low sensitivity to UV light.[155]

Regarding oxide nanocrystals for HTL applications, our group used NiO nanocrystals synthesized by the protecting-ligand assisted strategy.[25] The processing temperature can be as low as 130 °C, allowing us to integrate NiO-nanocrystal HTLs into flexible LEDs using MEH-PPV as emitters. The performance of the devices with NiO-nanocrystal HTLs was comparable to that of the control devices with PEDOT:PSS HTLs. Choy and co-workers demonstrated the application of post-treatment-free NiO_x nanoparticles as HTLs in OLEDs with poly[2-(4-(3′,7′-dimethyloctyloxy)-phenyl)-*p*-phenylene-vinylene] (P-PPV) as an emission layer.[24] Meyer and co-workers showed that MoO_3 films processed from nanoparticle suspensions acted as efficient HTLs, with electronic properties comparable to that of the films deposited *via* vacuum thermal evaporation.[156]

5.2 QLEDs

Colloidal QDs are solution-processable inorganic semiconductor nanocrystals with unique size-dependent properties and inherent

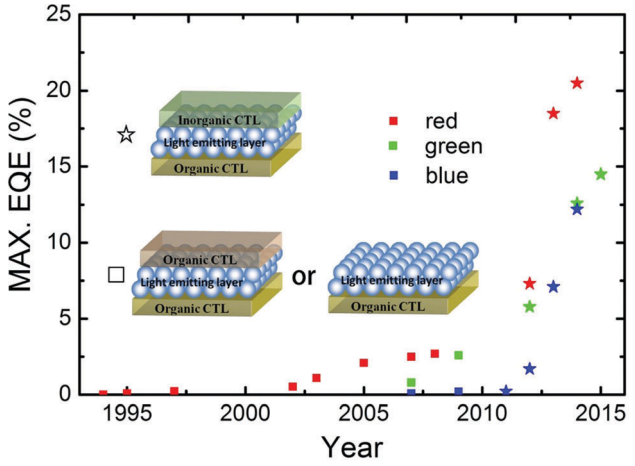

Fig. 12 Progression of peak EQEs over time for red, green and blue QLEDs. The corresponding device structures are also shown (ref. 18, 21, 46 and 159–175).

photo-physical stability. The narrow emission line-widths of QDs promise saturated color emission, making QLEDs extremely attractive for display applications.[157,158] Remarkable progress has been made regarding the efficiency of QLEDs in the past few years (Fig. 12).[18,21,46,159–175] Currently the maximum EQEs for red, green and blue QLEDs have reached 20.5%, 14.5% and 12.2%, respectively.[18,21,175] The red and green devices have exhibited long lifetimes of over 100 000 h and 90 000 h at an initial brightness of 100 cd m^{-2}, respectively.[18,21] This encouraging progress is attributable to steady efforts devoted to both materials chemistry of QDs and CTL materials and development of new device structures.

During the past ~20 years, the synthetic chemistry of colloidal QDs has advanced substantially, allowing superior control of their emission properties.[3,176–179] For example, for the most well developed system of CdSe/CdS core/shell dots, near-unity photoluminescence quantum yield and intrinsically mono-exponential decay were demonstrated.[177,179] Photoluminescence blinking of a single colloidal QD switching between several bright states and dark state under optical excitation can now be suppressed down to ~10^{-5} per photon absorption.[179,180] These developments provide a solid foundation for high-performance QLEDs.

The first QLED was reported by the Alivisatos group in 1994.[159] The device comprised a layer of organic PPV, a layer of CdSe QDs and two metal electrodes. In this simple device structure, the injected charges cannot be confined within QDs. Emissions from both QDs and PPV were observed. Later in 2002, the Bulović group invented a new device structure by sandwiching a QD emissive layer between two organic small-molecule CTLs to separate the luminescence process and the charge transport process.[162] The EQE of QLEDs based on this device structure can be optimized to ~2.5%.[164] However, the turn-on voltage, maximum brightness and power efficiency of the QLEDs were limited by the moderate conductivity of organic CTLs. The poor environmental stability of organic CTLs resulted in short lifetime of the QLEDs. In order to solve these problems, the Bulović group started to explore the possibility of replacing organic CTLs with inorganic oxide CTLs. In 2006, Caruge *et al.* introduced p-type NiO as HTLs.[48] Later on, they demonstrated all-inorganic QLEDs by utilizing sputtered ZnO/SnO_2 complex films and NiO films as ETLs and HTLs, respectively.[181] The all-inorganic QLEDs were capable of high-current-density operation. However, the sputtering process of metal oxides caused permanent damage to the optical properties of QD films. As a result, the EQEs of these all-inorganic QLEDs were less than 0.1%.

In 2008, an interesting report by Janssen *et al.* demonstrated all-solution-processed multilayer QLEDs (except the top electrodes) using ZnO nanocrystals as ETLs and organic materials as HTLs.[182] The colloidal ZnO nanoparticles were dispersed in isopropanol. Therefore the deposition of the ZnO layers did not dissolve all the underlying layers, which was critical for the fabrication of top CTLs. Although the device efficiency was rather poor, the turn-on voltage of the device with the ZnO layer was much lower than that of the device without the ZnO layer. This result implied a minimal electron injection barrier between the ZnO-nanocrystal ETLs and the QDs. Qian *et al.* greatly improved the performance of QLEDs using this hybrid device structure by optimizing the material choice of HTLs and the thickness of each layer in the device.[171] Maximum luminance and EQE values of 4200 cd m^{-2} and 0.22%, 68 000 cd m^{-2} and 1.8%, and 31 000 cd m^{-2} and 1.7% for blue, green and orange-red emission were achieved, respectively. In addition, these devices exhibited relatively good environmental stability, with lifetime at an initial brightness of 600 cd m^{-2} exceeding 250 h in low vacuum. These high-efficiency and bright devices indicated the great potential of this hybrid structure for QLEDs. From then on, ETLs based on colloidal ZnO nanocrystals were used in almost all high-efficiency QLEDs.[18,21,46,175]

Balanced charge injection is critical for the efficiency and lifetime of QLEDs. The use of ETLs based on colloidal ZnO nanocrystals significantly improved the electron injection efficiency. However, for most hybrid-structured QLEDs with CdSe or CdS emitters, hole injection is difficult because of the high ionization potential of the inorganic emitters. Furthermore, the electron mobility of ZnO ETLs can reach an order of 10^{-3} cm^2 $(V\ s)^{-1}$, which is much higher than the hole mobility of typical organic HTLs.[18] Achieving balanced charge injection became the top priority for high-performance QLEDs. One approach to improve hole injection is by adapting vacuum-deposited HTLs which are relatively well-developed in the small-molecule OLED industry.[46,172] In an inverted structure, ZnO nanocrystals were deposited onto ITO substrates as bottom ETLs. Kwak *et al.* compared a few small-molecule HTLs and concluded that HTLs with deeper highest-occupied-molecular-orbital (HOMO) levels were favourable for hole injection.[172] Kazlas and co-workers used doped small-molecule bilayers of 2,2′,7,7′-tetrakis[*N*-naphthalenyl(phenyl)-amino]-9,9-spirobifluorene (spiro-2NPB) and LG101 as HTLs to fabricate QLEDs. They showed that high-efficiency QLEDs with an EQE of 18% and a luminous power efficiency of 25 lm W^{-1} could be realized by controlling the distance of the recombination zone from the QD/ZnO nanocrystal interface.[46] Nevertheless, the efficiency roll-off characteristics and

lifetime of this device were still unsatisfactory. Our group introduced a conceptually new device structure by inserting an insulating layer between the QD layer and the ZnO-nanocrystal ETL (Fig. 13A).[18] We found that although bilayer-structured HTLs of poly(*N*,*N*′-bis(4-butylphenyl)-*N*,*N*′-bis(phenyl)-benzidine) (poly-TPD) and poly(9-vinylcarbazole) (PVK) could take advantage of the deep HOMO energy level of PVK and relatively high hole mobility of poly-TPD to realize better hole injection, electron injection into the QD layer was still in excess. The insertion of an insulating poly(methyl methacrylate) (PMMA) layer with a carefully engineered thickness blocked excess electron injection and improved charge balance in the device. Moreover, the PMMA layers preserved the superior emissive properties of QDs by modifying the interfacial interactions of QD/ZnO and maintaining the charge neutrality of the QD emitters. The champion device exhibited high EQEs of up to 20.5% and low efficiency roll-off (Fig. 13B and C). The operational lifetime of the PMMA-inserted devices reached more than 100 000 hours at an initial brightness of 100 cd m^{-2}, which is 1–2 orders longer than previous results (Fig. 13D). The strategy of inserting an insulating layer between the QD layer and the oxide ETLs was adopted by many follow-up studies.[183,184]

For QLEDs based on alternative QD emitters with relatively low electron affinity, such as CuInS, CuInGaS or ZnCuInS QDs, the band structure of ZnO ETLs needs to be tailored to improve electron injection. Alloying provides an effective approach to tune the electronic structures and properties of ZnO nanocrystals. For example, Kim *et al.* fabricated QLEDs with CuInS, CuInGaS, or ZnCuInS QDs as emitters and $Zn_xMg_{1-x}O$ nanocrystals with varied doping concentrations as ETLs.[185] The efficiency and maximum brightness of the devices increased substantially when the ratio of Mg in the oxide-nanocrystal ETLs increased from 0 to 10%. The authors suggested that alloying with Mg ions led to a reduced electron injection barrier at the interface of QD/oxide and hence improved device performance.

The idea of using solution-processed oxide CTLs to construct all-inorganic QLEDs is tempting. Currently p-type oxides, such as NiO, or n-type oxides with high work functions, such as WO_x and MoO_3, are used to replace PEDOT:PSS, one component of the multi-layer polymeric HTLs.[186–190] However, the direct contact of QDs with these oxides causes severe quenching of the QD emission. More detailed studies are necessary to guide the control of interfacial interactions between the QDs and the oxide HTLs.

5.3 Perovskite LEDs

Organic–inorganic hybrid perovskites (Fig. 14A), such as $CH_3NH_3PbI_3$ ($MAPbI_3$) and $NH_2CH{=}NH_2PbI_3$ ($FAPbI_3$), can be

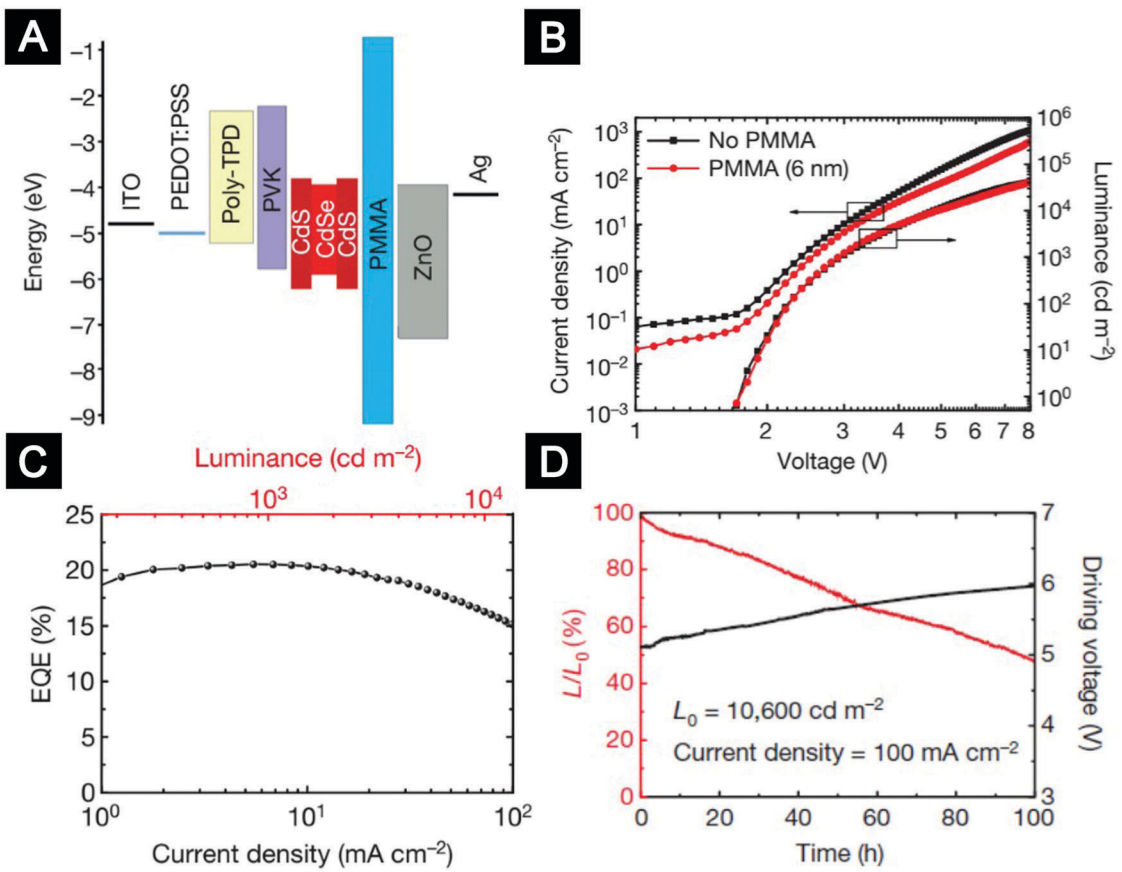

Fig. 13 Multilayer QLEDs with an insulting layer between the QD layer and the ZnO ETL. (A) Flat-band energy level diagram. (B) Current density and luminance *versus* voltage characteristics for QLEDs without or with the PMMA layer. (C) EQE *versus* current density and luminance for the device with the best efficiency. (D) Stability data for a QLED device (L, luminance). Figures reprinted with permission from ref. 18. Copyright 2014 Macmillan Publishers Limited.

processed from solutions at low temperatures to form crystalline direct-bandgap semiconductor films. Hybrid perovskite films may exhibit high photoluminescence quantum efficiency and good charge mobility, making them promising for electroluminescence applications.[191–193] One unique feature of perovskite emission is that the efficiency rises with increasing excitation level, which is different from that of the QDs or organic materials. Nevertheless, the stability issues of hybrid perovskite materials, for example, ion migration under a high electric field, need to be addressed to improve the LED lifetime.

Room-temperature perovskite electroluminescence was first reported by Tan *et al.* in 2014[192] (Fig. 14B). In the past two years, owing to the rich experience of interfacial engineering gained from other solution-processed LEDs, the EQEs of perovskite LEDs have improved dramatically, from 0.78% to 11.7%.[23,192–195] The key to achieving high-efficiency perovskite electroluminescence is integrating perovskite films with good emissive properties and full surface coverage into a LED structure, which can confine the injected charges within the perovskite layer to allow efficient radiative decay. For the 3D perovskite materials, such as $MAPbI_3$ and $FAPbI_3$, the formation of perovskite films is known to be very sensitive to the surface properties of the underlying layers. Our group employed PEI molecules to modify the surfaces of ZnO-nanocrystal films (Fig. 14C).[193] This interfacial engineering approach provided a high-energy hydrophilic surface to facilitate formation of high-quality perovskite thin films. Furthermore, the PEI modification lowered the work function of the ZnO-nanocrystal films, improving electron injection into the hybrid perovskite films. These two merits substantially improved device performance, leading to perovskite LEDs with an EQE of $\sim$3.5% at a high radiance of 28 W sr^{-1} m^{-2} and a low voltage of 2.2 V. In a later work, the ETLs of PEI-modified ZnO-nanocrystal films were inherited by our collaborators, the Wang and Huang group. They introduced perovskite emitters with structures of self-organized multiple quantum wells (MQWs) to replace the 3D perovskite films (Fig. 14D).[23] In the perovskite MQW films, the excited states were well confined in the lower-bandgap regions with excellent emissive properties, resulting in very efficient radiative decay. Together with the efficient electron injection provided by the PEI-modified ZnO ETLs, the MQW-based LEDs exhibited a record-high EQE of up to 11.7% and an exceptionally high power conversion efficiency of 5.5% at a current density of 100 mA cm^{-2}.

6. Recent developments of CTLs based on colloidal oxide nanocrystals for solution-processed solar cells

6.1 Organic solar cells

There has been a steady increase in the efficiencies of organic solar cells in the past decade.[196–200] Typically, organic solar cells rely on a BHJ structure, blends of electron donors and

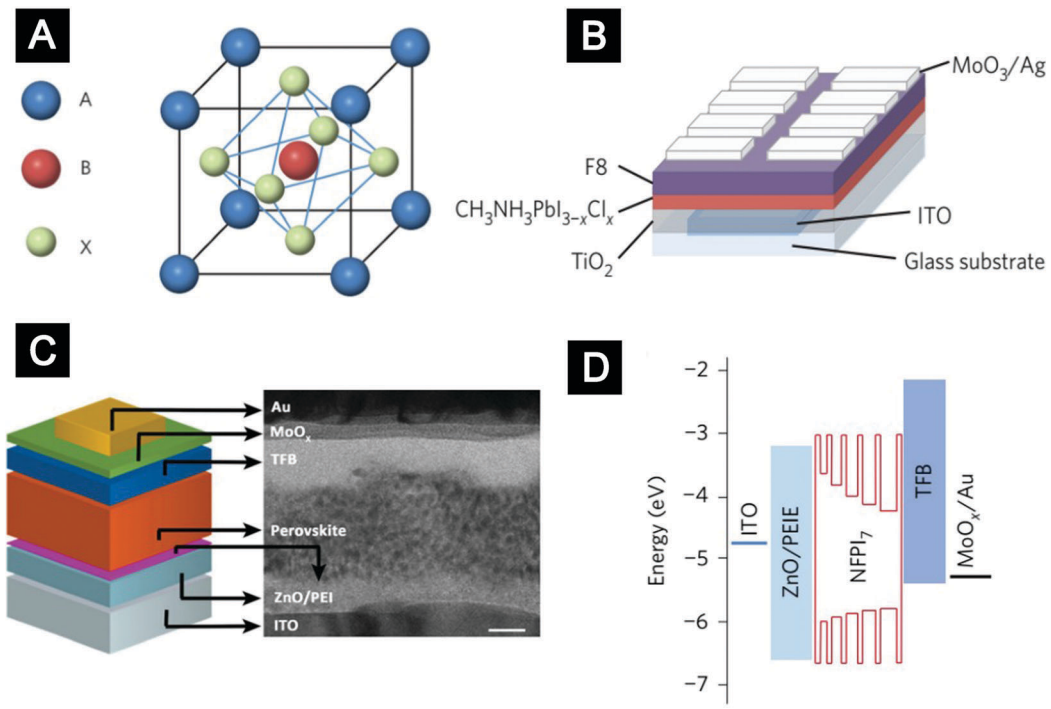

Fig. 14 (A) A single unit cell of an ABX_3 perovskite crystal, where A is methylammonium or formamidinium, B is Pb and X is I, Br or Cl. (B) Device structure of the first room-temperature perovskite LED. (C) A cross-sectional TEM image showing the architecture of the perovskite LED with PEI modified ZnO nanocrystals as ETLs. (D) Flat-band energy level diagram of the perovskite LED with self-organized multiple quantum wells as emitters and PEI modified ZnO nanocrystals as ETLs. (A and B) Reprinted with permission from ref. 192. Copyright 2014 Macmillan Publishers Limited. (C) Reprinted with permission from ref. 193. Copyright 2015 Wiley-VCH. (D) Reprinted with permission from ref. 23. Copyright 2016 Macmillan Publishers Limited.

electron acceptors, to convert incident photons to separated charges. Developments of active layers by designing new materials, *e.g.* low-bandgap polymers and non-fullerene acceptors, and optimizing BHJ morphologies *via* various film-deposition methods have been the heart of organic solar cell research.[196,199,201–204] As discussed in Section 2, CTLs influence all the elementary processes of organic solar cells. The improved device performance is also largely attributed to the evolution of device structures and interfacial engineering.

Currently organic solar cells can be divided into conventional and inverted architectures according to the polarity of charge collection and the direction of charge flow. For both architectures, oxide CTLs have been extensively studied to improve both power-conversion efficiency (PCE) and long-term device stability. Here we focus on oxide CTLs deposited from nanocrystal solutions. We highlight that for the fabrication of top CTLs, oxide nanocrystals in alcohol solutions are highly desirable to minimize damage to the BHJ blends.

As wide-bandgap semiconductors with low work function, n-type TiO_x and ZnO films were widely used in organic solar cells as ETLs.[60,205–207] The first organic solar cell based on TiO_x-nanocrystal ETLs was reported by Yang and co-workers.[208] In the early studies, it was shown that a high density of trap states in TiO_x significantly affected device performance.[209,210] To solve this problem, several strategies were proposed to modify the TiO_x ETLs.[208,211,212] For example, Choy and co-workers demonstrated that electronic properties of the TiO_x-nanocrystal films could be improved by incorporating metal (Au or Ag) nanoparticles.[212] Under 560–600 nm illumination, plasmon excited hot electrons in the Au nanoparticles were injected into TiO_x films to fill the traps, resulting in significantly improved device performance. Doping TiO_x nanocrystals was another effective strategy to improve the interfacial contact properties. For example, Cs_2CO_3 has been used to dope the TiO_x nanocrystals, resulting in increased film conductivity and better contact properties between the ETLs and the metal cathode.[208] In a follow-up work, Yang and co-workers systematically investigated organic solar cells using ETLs deposited from pure TiO_x nanocrystals, Cs-doped TiO_x nanocrystals and ZnO nanocrystals.[213] They found that even after UV illumination, the resistance of the device based on pure TiO_x nanocrystals was larger than that of the devices based on Cs-doped TiO_x and ZnO nanocrystals.

The most widely used ZnO nanocrystals in organic solar cells are synthesized *via* hydrolysis under basic conditions. These ZnO nanocrystals can be dispersed in alcoholic solvents and thereby can be used as either top ETLs in the conventional structure or bottom ETLs in the inverted structure.[214–217] Jen and co-workers firstly employed ZnO nanocrystals to modify the ITO substrates and developed inverted organic solar cells with significantly improved environmental stability.[214] Ackermann and co-workers employed ZnO-nanocrystal films as top ETLs in a conventional structure and systematically investigated the relationship between the optical, morphological and electronic properties of the ZnO ETLs and device performance.[218] They suggested that the significantly improved device performance was mainly due to the hole blocking properties of ZnO-nanocrystal ETLs in combination with the reduced contact resistance and interfacial recombination of photo-generated charges (Fig. 15A).

Controllable doping generates ZnO nanocrystals with tuneable optoelectronic properties. In a recent work, Ackermann and co-workers reported a modified protocol for the synthesis of colloidal AZO nanocrystals.[215] Highly conductive AZO-nanocrystal ETLs with low surface roughness were obtained even at a low annealing temperature of 80 °C. The highly conductive ETLs not only improved the compatibility of organic solar cells with large-scale solution processing but also opened new opportunities for efficient coloured solar cells. Colour tuning from green to yellow could be achieved by using AZO with different thicknesses as optical spacers.

In addition to single-junction organic solar cells, colloidal ZnO nanocrystals were also used to construct interconnecting

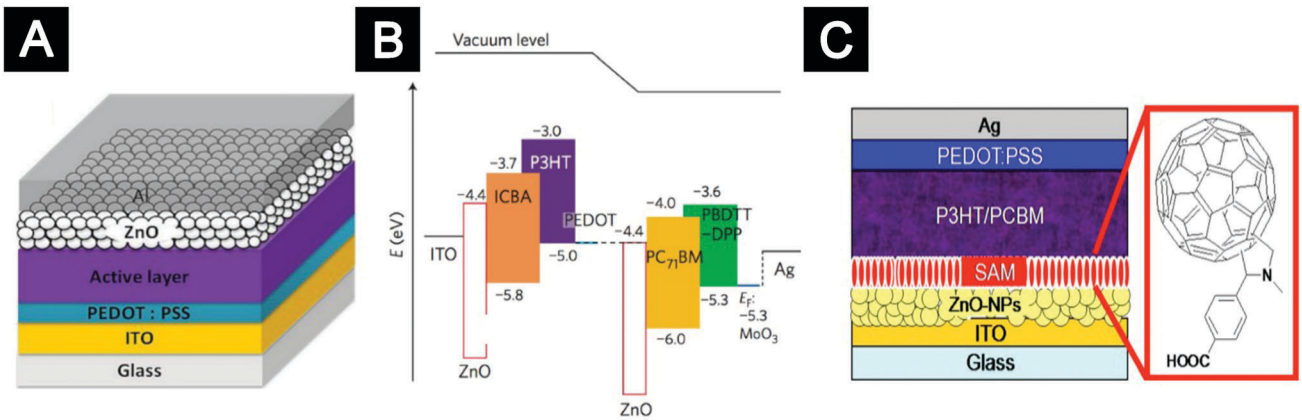

Fig. 15 Organic solar cells with ZnO nanocrystals as ETLs. (A) An organic solar cell with the conventional structure: ZnO-nanocrystal films as top ETLs. (B) Flat-band energy level diagram of a tandem organic solar cell with PEDOT:PSS and ZnO nanocrystals as ICL. (C) An organic solar cell with an inverted structure: fullerene-SAM modified ZnO nanocrystal films as bottom ETLs. (A) Reprinted with permission from ref. 218. Copyright 2014 Wiley-VCH. (B) Reprinted with permission from ref. 221. Copyright 2012 Macmillan Publishers Limited. (C) Reprinted with permission from ref. 230. Copyright 2008 American Institute of Physics.

layers (ICLs) and minimize loss of open-circuit voltage (V_{OC}) in tandem solar cells.[55,219–221] ICLs are sandwiched by two organic solar cell stacks and act as the charge recombination zone. ICLs generally consist of a p-type HTL and an n-type ETL, serving to shift vacuum level *via* alignment of the Fermi levels.[205,222] ZnO-nanocrystal layers with high conductivity can be obtained by low-temperature deposition procedures, which is desirable to minimize morphological changes of active layers used in bottom cells. By employing ZnO nanocrystal/PEDOT:PSS as the ICLs, Yang and co-workers demonstrated two-junction tandem solar cells with high PCEs of 8.6% and 10.6% (Fig. 15B).[219,221] In this tandem device, the V_{OC} was close to the sum of V_{OC} of two single junction cells with a negligible loss of $\sim$0.03 V. ICLs based on ZnO nanocrystals were also efficient for triple-junction tandem solar cells. By inserting two ICLs comprising ZnO nanocrystals, triple-junction polymer solar cells with a PCE of over 11% were fabricated.[223] Moreover, ZnO nanocrystals can form ideal ICLs not only with PEDOT:PSS but also with other materials, *e.g.* conjugated polyelectrolyte layers. Heeger and co-workers demonstrated a tandem device with a PCE of 8.6% based on the ZnO nanocrystals/conjugated polyelectrolyte ICLs.[224] Recently, a higher PCE of 11.3% was achieved by incorporating highly self-doped conjugated polyelectrolytes and ZnO nanocrystals as the ICLs.[225]

Despite the success of applying colloidal ZnO nanocrystals in single-junction and tandem organic solar cells, a major challenge lies in how to control intragap states induced by surface defects. It has been reported that surface defects of ZnO nanocrystals caused significant photocurrent loss and degraded charge selectivity of the cathode interface.[226,227] Prosa *et al.* showed that the release of oxygen chemisorbed onto the surfaces of ZnO nanocrystals under UV irradiation caused photo-induced shunts, resulting in reduced charge selectivity at the cathode interface.[228] This process represents an issue for the long-term photo-stability of organic solar cells. Riedl and co-workers showed that photo-induced shunting is a general phenomenon in neat and doped ZnO-based ETLs regardless of whether they are deposited from nanoparticle solutions or by vacuum deposition.[229] Several strategies to passivate the surface defects of ZnO-nanocrystal ETLs have been proposed. For example, Jen and co-workers introduced fullerene-based SAMs to avoid direct contact of ZnO nanocrystals with active layers (Fig. 15C).[230] Coordination polymers such as poly(ethylene oxide) (PEO) and poly(ethylene glycol) (PEG) were also used to passivate surface defects of ZnO nanocrystals, leading to improved device performance.[231–233] So and co-workers showed that UV-ozone treatment efficiently passivated the defect states of ZnO nanocrystals, as indicated by the suppression of defect emission in the photoluminescence measurements.[227] In a recent work, we developed a facial EDT treatment to modulate the intragap states of ZnO-nanocrystal films. The covalent bonding of EDT molecules onto ZnO nanocrystals removed a large fraction of the surface defects and introduced a new intragap band, resulting in enhanced electron transport and minimized interfacial bimolecular recombination loss of the resulting solar cells.[19] In addition, the well-passivated ZnO nanocrystals were less susceptible to oxygen and water molecules and hence further improved the ambient stability of obtained devices.

HTLs based on high work-function and n-type oxide nanocrystals, such as MoO_x and WO_x, have also been explored for organic solar cells.[156,234–236] For example, Lee *et al.* developed a facile approach to synthesize MoO_x nanocrystals based on a microwave-assisted method.[234] The devices with MoO_x-nanocrystal HTLs exhibited PCEs comparable to those of devices with PEDOT:PSS HTLs. In a recent report, low-temperature solution-processed WO_3 nanocrystals were employed as HTLs in organic solar cells by Brabec and co-workers.[235] The small WO_3 nanocrystals were stabilized in alcohol-based solvents. Smooth WO_3-nanocrystal films were obtained after a mild thermal annealing process (80 °C for 5 min), making them compatible with conventional and inverted organic solar cells. HTLs based on V_2O_5 nanocrystals and mixed-oxide nanocrystals of WO_3 and V_2O_5 have also been introduced to improve the device performance.[236] It was shown that the mixed oxide nanocrystals could effectively suppress the leakage current and enhance optical absorption, resulting in more efficient and stable devices.

Solution-processed p-type NiO_x films with high work function can function as hole transporting and electron blocking layers simultaneously in organic solar cells.[237,238] Recently, we applied pure NiO nanocrystals synthesized by the ligand-protection strategy to the fabrication of HTLs.[25] UV-ozone treatment was used to remove the insulating surface ligands and increase the work function of NiO films (Fig. 16A–D). The devices with NiO-nanocrystal HTLs exhibited an average PCE of 6.1%. In contrast, the average PCE for the devices with PEDOT:PSS as HTLs was 5.0%. In a recent report, Choy and co-workers reported a novel approach for the synthesis of nonstoichiometric NiO_x nanocrystals.[24] After carefully controlled calcination (270 °C for 2 h) in air, the obtained dark-black NiO_x nanocrystals were well dispersed in water to form a stable solution. Even without any post-deposition treatment, the HTLs based on NiO_x nanocrystals offered a high work function of 5.25 eV, providing excellent contact for most donor materials in organic solar cells (Fig. 16E and F).

6.2 QDSCs

Colloidal QDs are attractive for solar cells because of the unique combination of solution-processable characteristics, size-dependent electronic structure, excellent absorption in the visible and infrared region, and potential multi-exciton generation.[239–242] In the early stages, QDSCs adopted the Schottky structure, in which QDs were sandwiched between ITO and a low-work-function metal, such as Al and Mg.[243–246] However, the Schottky-structured devices suffered from low V_{OC} due to Fermi-level pinning at the Schottky interfaces, as well as inefficient carrier collection because most of the photo-excitations occurred at the regions away from the junction side. The evolution of a Schottky structure to a depleted-heterojunction device with n-type metal oxides as ETLs effectively increased the built-in electric field, giving rise to much improved device performance.[239,247] In recent years, the PCEs

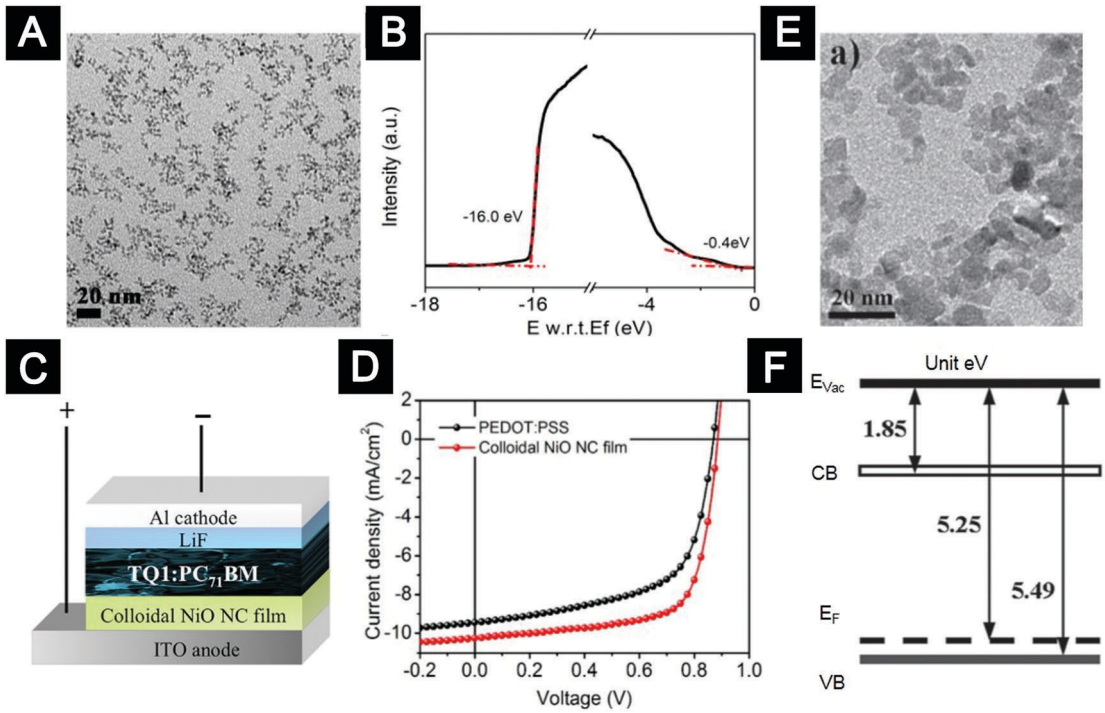

Fig. 16 P-type NiO_x nanocrystals and their application as HTLs in organic solar cells. (A) A typical TEM image of the colloidal NiO nanocrystals synthesized by the ligand-protecting method. (B) UPS spectrum of the NiO-nanocrystal HTL. (C) Device structure of organic solar cells with NiO-nanocrystal HTLs and (D) the corresponding *J*–*V* curves of the devices. (E) A typical TEM image of the NiO_x nanoparticles synthesized by the chemical precipitation method and (F) energy-level diagram of the NiO_x-nanocrystal HTL without any post-deposition treatment. (A–D) Reprinted with permission from ref. 25. Copyright 2014 American Chemical Society. (E–F) Reprinted with permission from ref. 24. Copyright 2015 Wiley-VCH.

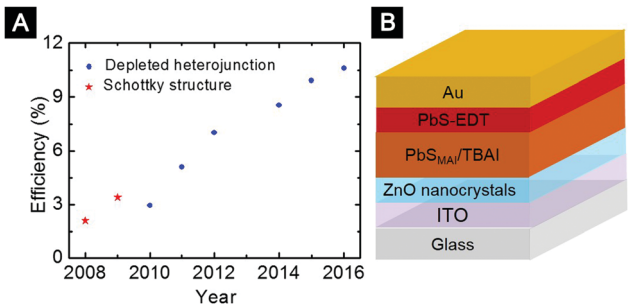

Fig. 17 (A) Progression of the PCE of QDSCs over time (ref. 22, 245 and 247–252). The PCEs of QDSCs with depleted-heterojunction structures are certified values. (B) Device architecture of the QDSC achieving the highest certified PCE to date. (B) Adapted with permission from ref. 22. Copyright 2016 American Chemical Society.

of QDSCs have shown steady improvements (Fig. 17A), owing to both surface engineering of QDs and optimization of oxide ETLs.[22,241,245,247–254] The structure of the device with the highest certified PCE of 10.6% is shown in Fig. 17B. For this device, ZnO-nanocrystal films were used as ETLs.[22]

The compositions and surface coordination states of QDs, which heavily rely on the synthesis, purification and processing procedures, have significant impacts on carrier mobility, defect density, as well as doping density of the QD films. Exquisite modulations of synthetic and purification procedures are important for improving the performance of QDSCs.[254–256] Ligand engineering of QDs can effectively reduce defect density and suppress carrier recombination in the QD films, as well as tune the absolute energy levels. For example, halide ligands were explored for passivation of surface defects, leading to QD films with higher carrier mobility and thereby much improved device performance.[250] The Bawendi group showed that the ligand-induced surface dipoles could influence the absolute energy levels of QD films.[117,251] This finding made it appealing to tailor the band energy alignment of the QD layers with carefully engineered ligands.

For heterojunction QDSCs, the n-type oxide layer is critical to determine the thickness of the depletion region in the QD layer, the built-in voltage, as well as electron extraction and transport. In the early stages, TiO_2 paste composed of nanocrystals with sizes of $\sim$20 nm and carrier density of $\sim 10^{16}$ cm^{-3} was utilized for ETL fabrication.[241] A PCE of over 5% was achieved. Both the V_{OC} and the short-circuit current (J_{SC}) were enhanced compared to the device with Schottky structure. For the heterojunction QDSCs, the energy level offset between the conduction band of TiO_2 and QDs should be favourable to facilitate electron extraction from QDs to TiO_2 while avoiding excess loss of V_{OC}. For example, the Sargent group studied QDSCs using two types of TiO_2 ETLs, one made from nanocrystals with an electron affinity of -3.8 eV and another one deposited by sputtering with an electron affinity of -4.0 eV.[257] The parameters of QDSCs based on nanocrystals and sputtered TiO_2 thin film were 0.7 and 0.61 V for V_{OC}, 3.5% and 2.7% for PCE, respectively.

Given that the electron affinity of QDs used in the devices is ~3.6 eV, the authors suggested that the energy-level offset of 0.2 eV favoured electron injection from QDs to TiO_2 nanocrystal thin films.[257] For the sputtered TiO_2 thin film, the deeper TiO_2 band-edge compromised the V_{OC}.

Interfacial recombination is an important loss pathway that may limit J_{SC} and degrade device efficiency.[258] Sargent and co-workers showed that inserting a buffer layer of ZnO onto the surface of TiO_2 effectively reduced interfacial recombination, leading to remarkably improved device performance.[255] This work suggests that defect centers in TiO_2 are one limiting factor for device performance. This work also implies that ZnO may outperform TiO_2 in terms of suppressing interfacial recombination.

Currently the majority of the state-of-the-art high-efficiency QDSCs use solution-processed ZnO, *e.g.* ZnO-nanocrystal films, as ETLs.[20,22] The relationship between the properties of ZnO-nanocrystal ETLs and device performance has been investigated by a number of studies. For example, in a QDSC with an inverted structure, effects of varying the doping density of the ZnO-nanocrystal films by illumination were explored.[256] Under UV illumination, the absorbed gas molecules, for example O_2, on the surfaces of ZnO nanocrystals were removed, resulting in enhanced doping density. Consequently, an additional portion of the depletion region was formed within the hole accepting PbS layer. These effects led to a transition from excitonic behavior to p–n behavior in the device, leading to enhanced charge generation and extraction. In another work, Azmi and co-workers applied the EDT surface passivation method developed by our group to the ZnO-nanocrystal ETLs used in QDSCs.[259] They confirmed that the intragap trap states originating from the notorious oxygen-deficient surface states of the ZnO nanocrystals were effectively removed after the EDT treatment. This treatment suppressed interfacial charge recombination at the QD/ETL heterojunction and the PCE was improved from 9.45 to 10.26%. Very recently, Kim *et al.* showed that addition of organic molecules with strong dipole moment decreased the work function of the ZnO layer, giving rise to increased built-in voltage and better device performance.[20] As a result, a remarkable PCE of 10.7% was obtained.

6.3 Perovskite solar cells

Metal halide perovskite solar cells have attracted worldwide attention in recent years due to their high efficiencies and low processing cost.[260–266] Owing to the rapid developments of perovskite materials, film deposition and processing and interfacial engineering, the efficiencies of perovskite solar cells have rocketed from the first reported 3.8% to a certified 22.1% over the past few years. Some recent works, such as using cesium ions along with formamidinium cations in lead bromide–iodide cells and two-dimensional Ruddlesden–Popper perovskite solar cells, have shed light on addressing critical factors of thermal- and photo-stability under operating conditions.[267,268]

Initial studies of perovskite solar cells focused on a device structure similar to dye-sensitized solar cells with mesoporous TiO_2 or Al_2O_3 as the scaffolds.[6,269] High temperature (450–500 °C) sintered compact TiO_2 layers were often used. Further investigation revealed that perovskite materials exhibited ambipolar charge transport and long charge diffusion length, resulting in the success of perovskite solar cells with simplified planar heterojunction (PHJ) structures, in which the perovskite layer was sandwiched between ETL and HTL.[270–273] Various CTLs developed for other solution-processed optoelectronics were demonstrated to be suitable for perovskite solar cells. Among them, CTLs based on colloidal oxide nanocrystals showed great potential. Depending on selective charge extraction and transport properties of the bottom contacts, the PHJ solar cells can be further divided into two sub-categories, conventional (n–i–p) and inverted (p–i–n) structure.[274] In this section, we will discuss a few relevant examples.

The first PHJ perovskite solar cell developed by Snaith and co-workers was based on high-temperature-sintered compact TiO_2 ETLs by gradually decreasing the thickness of Al_2O_3 scaffolds used in mesoporous devices.[6] By employing high-conductivity yttrium-doped TiO_2 nanocrystals as ETLs, Yang and co-workers demonstrated one of the most efficient planar devices based on TiO_2 ETLs.[263] The yttrium doping increased the conductivity of TiO_2-nanocrystal films from 6×10^{-6} to 2×10^{-5} S cm^{-1} and significantly improved charge transport in the devices. By further reducing the work function of ITO substrates with PEIE and controlling the humidity of the annealing atmosphere, planar devices with the best PCE of 19.3% and an average PCE of 16.6% were obtained. In addition to TiO_2 nanocrystals, ZnO nanocrystals were also employed as ETLs in conventional planar perovskite solar cells. Liu *et al.* first introduced ZnO nanocrystals as the ETLs for the fabrication of efficient perovskite solar cells at low temperatures (Fig. 18A).[275] Highly conductive crystalline SnO_2 and Zn_2SnO_4 (ZSO) nanocrystals were also used as efficient ETLs in conventional PHJ perovskite solar cells.[276,277] For example, Rao *et al.* employed SnO_2 nano-colloids to deposit ETLs for PHJ perovskite solar cells.[278] Compared to the TiO_2, the SnO_2 ETLs exhibited higher mobility, resulting in improved photocurrent and device performance. Recently, Seok and co-workers fabricated PHJ perovskite solar cells by employing ETLs deposited from highly dispersed ZSO nanocrystal solutions.[277,279] A relatively low temperature (100 °C) was sufficient to obtain ZSO-nanocrystal films with high electron mobility. Moreover, due to its low refractive index, the insertion of the ZSO layer further improved the transmittance of substrates in the visible regions. Based on the high-quality ZSO ETLs, flexible perovskite solar cells with a PCE of ~15% were achieved.[277] By further tailoring the energy level and electron transporting properties of ZSO ETLs using nanocrystals with different sizes, the loss of photogenerated electrons was further reduced. An improved PCE of ~16% was achieved for the devices based on flexible substrates.[279]

Currently a critical issue at the interfaces of oxide/perovskite is the lack of control over the sensitive surface states of the oxide nanocrystals. For example, it was shown that oxygen vacancy due to the light-induced desorption of surface absorbed oxygen in TiO_x films accounted for poor stability of TiO_2-based devices.[280] For devices based on ZnO ETLs, surface

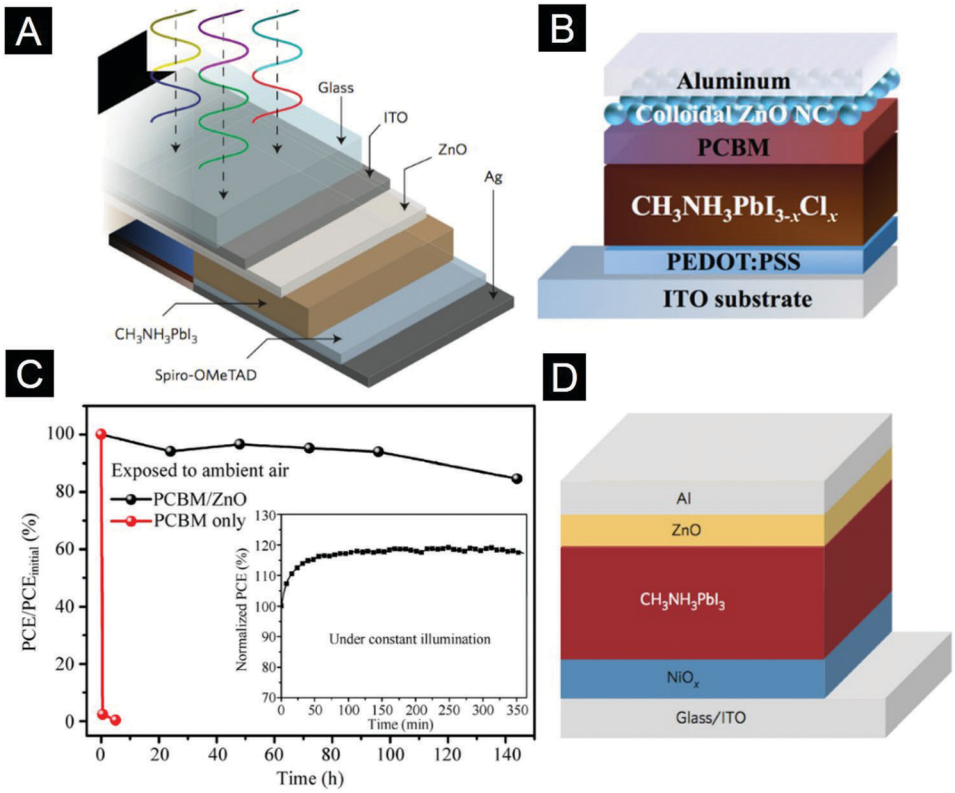

Fig. 18 (A) Conventional device structure of the perovskite solar cell with ZnO nanocrystals as ETL. (B) Device structure of the inverted planar perovskite solar cell with a ZnO-nanocrystal layer between the PCBM layer and the electrode. (C) Normalized PCE characteristics of the devices as a function of exposure time in air. The inset indicates no degradation of the PCEs when the un-encapsulated device was tested in air under constant illumination for 6 h. (D) Device structure of the perovskite solar cell with NiO_x and ZnO as HTL and ETL, respectively. (A) Reprinted with permission from ref. 275. Copyright 2014 Macmillan Publishers Limited. (B and C) Reprinted with permission from ref. 17. Copyright 2014 Tsinghua University Press and Springer. (D) Reprinted with permission from ref. 294. Copyright 2014 Macmillan Publishers Limited.

hydroxyl groups and acetate ligands at the surfaces of oxide nanocrystals may cause unwanted reactions with perovskite films, degrading the stability of perovskite solar cells. The intragap states of the oxide-nanocrystal films can lead to charge accumulation at the cathode interfaces and generate anomalous hysteresis in the *J–V* curves.[281,282] Further efforts are necessary to investigate the surface passivation of oxide-nanocrystal ETLs for perovskite solar cells.

To solve the hysteresis issue of perovskite solar cells, one feasible approach is to use the inverted planar device structure (p–i–n structure). It was shown that fullerene-based ETLs with no dangling bonds or surface states, such as (6,6)-phenyl C_{61}-butyric acid methyl ester ($PC_{61}BM$) and indene-C_{60} bis-adduct (ICBA), could efficiently suppress hysteresis, leading to improved device performance.[283] However, the $PC_{61}BM$ films cannot form stable contact with the low-function metal electrodes. Inserting additional buffer layers between $PC_{61}BM$ and the cathode electrodes was essential to improve the device efficiency and stability. Snaith and co-workers firstly modified the cathode interface with a TiO_x layer to fabricate air-stable inverted PHJ perovskite solar cells.[284] However, the obtained devices needed to be activated under constant light illumination for several minutes to obtain high PCEs. Moreover, the annealing temperature of $\sim$130 °C for TiO_x films caused decomposition of the underneath perovskite layer. To preserve the superior electronic properties of perovskites, we introduced room-temperature deposited ZnO-nanocrystal interlayers between $PC_{61}BM$ and metal electrodes (Fig. 18B).[17] The obtained devices exhibited a significantly enhanced PCE of 15.9% and excellent air stability, while the control devices without ZnO-nanocrystal layers degraded utterly after exposure in air for 30 min (Fig. 18C). In addition to ZnO, highly conductive AZO-, ZSO- or SnO_2-nanocrystal films were used to achieve thicker buffer layers between $PC_{61}BM$ and metal electrodes.[285–287] Moreover, it has been demonstrated that thick oxide-nanocrystal films were effective in terms of protecting the underneath perovskite films during the sputtering process of the ITO electrode. Therefore these oxide nanocrystals can be used to fabricate perovskite tandem solar cells.[288]

One important direction in inverted perovskite solar cells is to achieve stable anode contact by replacing hygroscopic PEDOT:PSS with stable metal oxides. Examples include p-type metal oxides, such as CuO_x and NiO_x, and n-type metal oxides, such as WO_x and MoO_x.[289–293] It should be noted that processing of perovskite films on these metal oxide films requires careful control due to the fact that complicated interactions between these metal oxides and perovskites often lead to poor film quality. In many cases, a fast crystallization process induced by anti-solvent quenching was found to be beneficial

in terms of obtaining high-quality perovskite films. Up to now, NiO_x is the most widely investigated HTL in inverted perovskite solar cells. In a recent work by You *et al.*, inverted PHJ perovskite solar cells with NiO HTLs and ZnO-nanocrystal ETLs were fabricated (Fig. 18D).[294] These devices showed significantly improved stability against water and oxygen degradation, *i.e.* less than 10% degradation even after 6 days storage in air without encapsulation. NiO HTLs can also be deposited from nanocrystal solutions.[295,296] The devices based on NiO-nanocrystal HTLs exhibited high reproducibility with the best PCE of 17.6% and an average efficiency of 15.8%. The low processing temperature of the NiO-nanocrystal HTLs enabled the fabrication of flexible perovskite solar cells with a promising PCE of 14.5%.

7. Conclusions and prospects

Colloidal oxide nanocrystals offer a unique combination of excellent low-temperature solution processability, rich and controllable optoelectronic properties and intrinsic stability, which spurred their applications as CTLs for solution-processed solar cells and LEDs (Fig. 19). Fully exploiting the potential of CTLs based on oxide nanocrystals relies on both in-depth understanding of how the properties of CTLs impact device operation, some of which is currently unknown, to guide material design and on-demand development of material chemistry for colloidal oxide nanocrystals, some of which is currently unavailable, to allow processing of CTLs with desirable properties. The following aspects shall be paid more attention to in future research.

(i) Ligand chemistry of colloidal oxide nanocrystals. Knowledge of the ligand chemistry of colloidal oxide nanocrystals is surprisingly scarce despite the fact that surface tuning and modification are imperative for their CTL applications. As-synthesized oxide nanocrystals are often ill-suited for CTL applications. For example, weak-binding ligands used to stabilize oxide nanocrystals in solutions tend to dissociate from the nanocrystal surfaces during film processing and device operation, leaving unpassivated surfaces. The high-reactivity surfaces of oxide nanocrystals make the properties of CTLs very sensitive to environments, processing and operational history, which may deteriorate device stability.

We suggest that ligands with strong anchoring groups to facilitate their tight binding onto surfaces of oxide nanocrystals shall be used to lower surface activity and improve stability of the CTL films. The concept of entropy ligand is likely to be a key guideline to meet the demands of both stability of colloidal oxide nanocrystals in solution and charge transport of their corresponding CTLs. It is also possible to further modify the properties of oxide-nanocrystal CTLs by judicious molecular design of functional ligands.

Currently, establishing a link between surface structure of oxide nanocrystals and electronic/transport properties of the corresponding CTLs remains a crucial open question in this field. We highlight that investigations on ligand chemistry may provide unique opportunities to achieve complete surface passivation of the oxide nanocrystals, providing powerful tools to understand and manipulate the intragap states of the corresponding oxide CTLs. Techniques that have been successful in characterizing the intragap states of other semiconductors, such as thermal admittance spectroscopy, deep-level transient spectroscopy, drive-level capacitance profiling and photothermal deflection spectroscopy, may be useful in quantifying the intragap states of the oxide-nanocrystal CTLs.

(ii) Synthetic chemistry of p-type oxide nanocrystals. Up to now, the synthesis of NiO nanocrystals is one of the few examples for p-type oxide nanocrystals applicable as HTLs. Synthetic chemistry of NiO nanocrystals is not as mature as that of n-type oxide nanocrystals. Our studies indicated that the extinction coefficient of NiO-nanocrystal films was about one order of magnitude larger than that of other oxide-nanocrystal

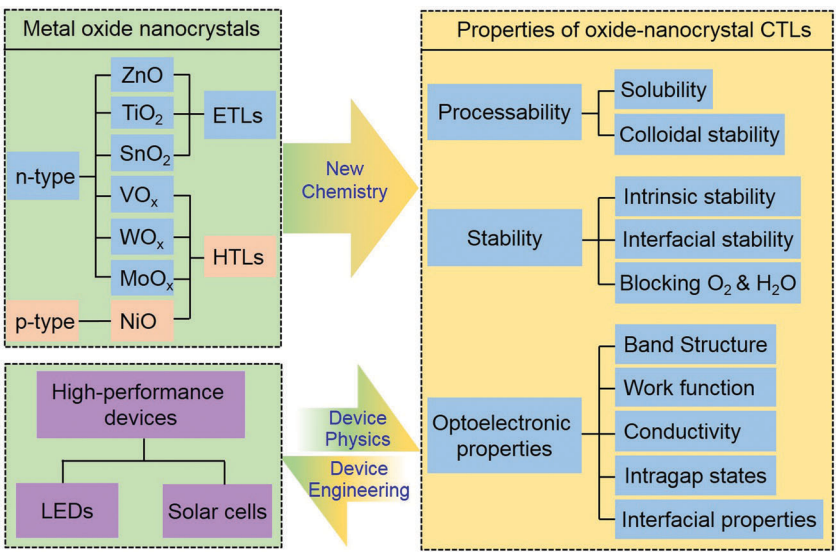

Fig. 19 Relationship between the chemistry of colloidal oxide nanocrystals, processing and properties of CTLs and device performance of solution-processed LEDs and solar cells.

CTLs, such as ZnO-nanocrystal films, which may cause unneglectable absorption of photons. More exquisite control over the band structure, carrier density, intragap states, stoichiometry and optical properties of the NiO-nanocrystal HTLs shall be pursued in the future. It is also of interest to develop the synthetic chemistry of other p-type oxide nanocrystals, such as the ternary Cu(I) delafossite oxides.

(iii) In-depth understanding of interactions between oxide-nanocrystal CTLs and active layers. Detailed mechanistic studies on interactions between oxide-nanocrystal CTLs and active layers under operational conditions are lacking despite the extensive practice of applying oxide nanocrystals as CTLs in solution-processed LEDs and solar cells. For example, quenching of excitons formed in the QDs by the adjacent oxide CTLs has been identified as one critical factor that limits device performance. However, quenching mechanisms under operational conditions have not been fully disclosed. In our laboratory, preliminary studies on the photoluminescence of QDs in contact with oxide-nanocrystal films showed that several quenching mechanisms, including photo-induced charge separation and charging of QDs due to interfacial charge transfer and energy transfer, were involved depending on the properties of both CTLs and QDs. Moreover, electric field and electric current should be taken into consideration when interpreting the quenching mechanism under electrically driven conditions. For instance, the electric field in the QD layer can modify the radiative recombination rate through spatial separation of the electron and the hole. Multiple techniques, including single-dot photoluminescence or electroluminescence spectroscopy, electrostatic force microscopy, transient-absorption spectroscopy and *in situ* photoluminescence–electroluminescence spectroscopy, should be combined to gain more comprehensive and rigorous understanding and to provide guidelines to exquisite design of oxide-nanocrystal CTLs beyond the state-of-the-art.

In summary, there is still plenty of room to boost device performance by developing new material chemistry of colloidal oxide nanocrystals and custom-tailoring the properties and processing of CTLs. These efforts shall lead to a new generation of high-performance and all-solution-processed solar cells and LEDs with both ETLs and HTLs based on colloidal oxide nanocrystals, which may revolutionize the current LED and solar-cell industry based on vacuum-deposited crystalline semiconductors. Furthermore, such knowledge can be transferred to the research of other solution-processed devices, such as contact engineering of solution-processed field-effect transistors.

Acknowledgements

This work was financially supported by the National Key Research and Development Program of China (2016YFB0401602 and 2016YFA0204000), the National Natural Science Foundation of China (51522209, 91433204, U1632118, and 21571129), the Fundamental Research Funds for the Central Universities (2015FZA3005), Shanghai Key Research program (16JC1402100), Shanghai International Cooperation Project (16520720700) and the Carl Tryggers Stiftelse and the Swedish Government Strategic Research Area in Materials Science on Functional Materials at Linköping University (Faculty Grant SFO-Mat-LiU # 2009-00971). S. B. is a VINNMER Fellow and Marie Skłodowska-Curie Fellow. We thank Prof. Jianpu Wang (Nanjing Tech University, China), Mr Zhenxing Zhang (Department of Chemistry, Zhejiang University, China), Mr Desui Chen (Department of Chemistry, Zhejiang University, China), Mr Yunzhou Deng (Department of Chemistry, Zhejiang University, China), Mr Yang Liu (School of Materials Science and Engineering, Zhejiang University, China) and Mr Fei Wang (School of Physic Science and Technology, Shanghai Tech University, China) for the assistance in preparing this manuscript.

References

1 J. H. Burroughes, A. R. Brown and R. N. Marks, *Nature*, 1990, **347**, 539–541.
2 R. H. Friend, R. W. Gymer, A. B. Holmes, J. H. Burroughes, R. N. Marks, C. Taliani, D. D. C. Bradley, D. A. Dos Santos, J. L. Bredas, M. Logdlund and W. R. Salaneck, *Nature*, 1999, **397**, 121–128.
3 D. J. Noms, C. B. Murray and M. G. Bawendi, *J. Am. Chem. Soc.*, 1993, **115**, 8706.
4 Y. D. Yin and A. P. Alivisatos, *Nature*, 2005, **437**, 664–670.
5 X. G. Peng, *Nano Res.*, 2009, **2**, 425–447.
6 M. M. Lee, J. Teuscher, T. Miyasaka, T. N. Murakami and H. J. Snaith, *Science*, 2012, **338**, 643–647.
7 H. S. Kim, C. R. Lee, J. H. Im, K. B. Lee, T. Moehl, A. Marchioro, S. J. Moon, R. Humphry-Baker, J. H. Yum, J. E. Moser, M. Gratzel and N. G. Park, *Sci. Rep.*, 2012, **2**, 591.
8 M. Singh, H. M. Haverinen, P. Dhagat and G. E. Jabbour, *Adv. Mater.*, 2010, **22**, 673–685.
9 B. J. de Gans, P. C. Duineveld and U. S. Schubert, *Adv. Mater.*, 2004, **16**, 203–213.
10 K. Hwang, Y. S. Jung, Y. J. Heo, F. H. Scholes, S. E. Watkins, J. Subbiah, D. J. Jones, D. Y. Kim and D. Vak, *Adv. Mater.*, 2015, **27**, 1241–1247.
11 C. W. Sele, T. von Werne, R. H. Friend and H. Sirringhaus, *Adv. Mater.*, 2005, **17**, 997–1001.
12 H. Sirringhaus, T. Kawase, R. H. Friend, T. Shimoda, M. Inbasekaran, W. Wu and E. P. Woo, *Science*, 2000, **290**, 2123.
13 B. H. Kim, M. S. Onses, J. B. Lim, S. Nam, N. Oh, H. Kim, K. J. Yu, J. W. Lee, J. H. Kim, S. K. Kang, C. H. Lee, J. Lee, J. H. Shin, N. H. Kim, C. Leal, M. Shim and J. A. Rogers, *Nano Lett.*, 2015, **15**, 969–973.
14 V. Wood, M. J. Panzer, J. Chen, M. S. Bradley, J. E. Halpert, M. G. Bawendi and V. Bulović, *Adv. Mater.*, 2009, **21**, 2151–2155.
15 J. H. Kim, S. T. Williams, N. Cho, C.-C. Chueh and A. K. Y. Jen, *Adv. Energy Mater.*, 2015, **5**, 1401229.
16 H. Zheng, Y. N. Zheng, N. L. Liu, N. Ai, Q. Wang, S. Wu, J. H. Zhou, D. G. Hu, S. F. Yu, S. H. Han, W. Xu, C. Luo, Y. H. Meng, Z. X. Jiong, Y. W. Chen, D. Y. Li, F. Huang,

J. Wang, J. B. Peng and Y. Cao, *Nat. Commun.*, 2013, **4**, 2885.
17 S. Bai, Z. W. Wu, X. J. Wu, Y. Z. Jin, N. Zhao, Z. H. Chen, Q. Q. Mei, X. Wang, Z. Z. Ye, T. Song, R. Y. Liu, S.-t. Lee and B. Q. Sun, *Nano Res.*, 2014, **7**, 1749–1758.
18 X. L. Dai, Z. X. Zhang, Y. Z. Jin, Y. Niu, H. J. Cao, X. Y. Liang, L. W. Chen, J. P. Wang and X. G. Peng, *Nature*, 2014, **515**, 96–99.
19 S. Bai, Y. Z. Jin, X. Y. Liang, Z. Z. Ye, Z. W. Wu, B. Q. Sun, Z. F. Ma, Z. Tang, J. P. Wang, U. Würfel, F. Gao and F. L. Zhang, *Adv. Energy Mater.*, 2015, **5**, 201401606.
20 G. H. Kim, F. P. Garcia de Arquer, Y. J. Yoon, X. Lan, M. X. Liu, O. Voznyy, Z. Y. Yang, F. J. Fan, A. H. Ip, P. Kanjanaboos, S. Hoogland, J. Y. Kim and E. H. Sargent, *Nano Lett.*, 2015, **15**, 7691–7696.
21 Y. X. Yang, Y. Zheng, W. R. Cao, A. Titov, J. Hyvonen, J. R. Manders, J. G. Xue, P. H. Holloway and L. Qian, *Nat. Photonics*, 2015, **9**, 259–266.
22 X. Z. Lan, O. Voznyy, F. P. Garcia de Arquer, M. X. Liu, J. X. Xu, A. H. Proppe, G. Walters, F. J. Fan, H. R. Tan, M. Liu, Z. Y. Yang, S. Hoogland and E. H. Sargent, *Nano Lett.*, 2016, **16**, 4630–4634.
23 N. N. Wang, L. Cheng, R. Ge, S. T. Zhang, Y. F. Miao, W. Zou, C. Yi, Y. Sun, Y. Cao, R. Yang, Y. Q. Wei, Q. Guo, Y. Ke, M. T. Yu, Y. Z. Jin, Y. Liu, Q. Q. Ding, D. W. Di, L. Yang, G. C. Xing, H. Tian, C. H. Jin, F. Gao, R. H. Friend, J. P. Wang and W. Huang, *Nat. Photonics*, 2016, **10**, 699–704.
24 F. Jiang, W. C. H. Choy, X. C. Li, D. Zhang and J. Q. Cheng, *Adv. Mater.*, 2015, **27**, 2930–2937.
25 X. Y. Liang, Q. Yi, S. Bai, X. L. Dai, X. Wang, Z. Z. Ye, F. Gao, F. L. Zhang, B. Q. Sun and Y. Z. Jin, *Nano Lett.*, 2014, **14**, 3117–3123.
26 N. Espinosa, R. García-Valverde, A. Urbina and F. C. Krebs, *Sol. Energy Mater. Sol. Cells*, 2011, **95**, 1293–1302.
27 F. C. Krebs, *Sol. Energy Mater. Sol. Cells*, 2009, **93**, 465–475.
28 S. G. Kwon and T. Hyeon, *Acc. Chem. Res.*, 2008, **41**, 1696–1709.
29 J. H. Lee, S. Zhang and S. H. Sun, *Chem. Mater.*, 2013, **25**, 1293–1304.
30 M. Niederberger, *Acc. Chem. Res.*, 2007, **40**, 793–800.
31 S. D. Lounis, E. L. Runnerstrom, A. Llordes and D. J. Milliron, *J. Phys. Chem. Lett.*, 2014, **5**, 1564–1574.
32 A. Kołodziejczak-Radzimska and T. Jesionowski, *Materials*, 2014, **7**, 2833–2881.
33 K. Zilberberg, J. Meyer and T. Riedl, *J. Mater. Chem. C*, 2013, **1**, 4796.
34 C.-C. Chueh, C.-Z. Li and A. K. Y. Jen, *Energy Environ. Sci.*, 2015, **8**, 1160–1189.
35 F. Z. Wang, Z. A. Tan and Y. F. Li, *Energy Environ. Sci.*, 2015, **8**, 1059–1091.
36 H. Kim, K.-G. Lim and T.-W. Lee, *Energy Environ. Sci.*, 2016, **9**, 12–30.
37 S. Chen, J. R. Manders, S.-W. Tsang and F. So, *J. Mater. Chem.*, 2012, **22**, 24202–24212.
38 K. Wang, C. Liu, T. Y. Meng, C. Yi and X. Gong, *Chem. Soc. Rev.*, 2016, **45**, 2937–2975.
39 Z. Q. Liang, Q. F. Zhang, L. Jiang and G. Z. Cao, *Energy Environ. Sci.*, 2015, **8**, 3442–3476.
40 G. Yang, H. Tao, P. L. Qin, W. J. Ke and G. J. Fang, *J. Mater. Chem. A*, 2016, **4**, 3970–3990.
41 W. C. Choy and D. Zhang, *Small*, 2016, **12**, 416–431.
42 W. Yin, L. J. Pan, T. B. Yang and Y. Y. Liang, *Molecules*, 2016, **21**, 837.
43 W. B. Yan, S. Y. Ye, Y. L. Li, W. H. Sun, H. X. Rao, Z. W. Liu, Z. Q. Bian and C. H. Huang, *Adv. Energy Mater.*, 2016, **6**, 1600474.
44 W. K. Bae, Y. S. Park, J. Lim, D. Lee, L. A. Padilha, H. McDaniel, I. Robel, C. Lee, J. M. Pietryga and V. I. Klimov, *Nat. Commun.*, 2013, **4**, 2661.
45 C. Javaux, B. Mahler, B. Dubertret, A. Shabaev, A. V. Rodina, L. EfrosAl, D. R. Yakovlev, F. Liu, M. Bayer, G. Camps, L. Biadala, S. Buil, X. Quelin and J. P. Hermier, *Nat. Nanotechnol.*, 2013, **8**, 206–212.
46 B. S. Mashford, M. Stevenson, Z. Popovic, C. Hamilton, Z. Zhou, C. Breen, J. Steckel, V. Bulovic, M. Bawendi, S. Coe-Sullivan and P. T. Kazlas, *Nat. Photonics*, 2013, **7**, 407–412.
47 K. Tvrdy, P. A. Frantsuzov and P. V. Kamat, *Proc. Natl. Acad. Sci. U. S. A.*, 2011, **108**, 29–34.
48 J. M. Caruge, J. E. Halpert, V. Bulovic and M. G. Bawendi, *Nano Lett.*, 2006, **6**, 2991–2994.
49 L. A. Pettersson, L. S. Roman and O. Inganäs, *J. Appl. Phys.*, 1999, **86**, 487.
50 F. Gao, *Loss Mechanisms in Bulk Heterojunction Organic Photovoltaics*, University of Cambridge, 2011.
51 B. A. MacLeod, N. E. Horwitz, E. L. Ratcliff, J. L. Jenkins, N. R. Armstrong, A. J. Giordano, P. J. Hotchkiss, S. R. Marder, C. T. Campbell and D. S. Ginger, *J. Phys. Chem. Lett.*, 2012, **3**, 1202–1207.
52 M. T. Greiner and Z.-H. Lu, *NPG Asia Mater.*, 2013, **5**, e55.
53 F. X. Xie, W. C. Choy, C. D. Wang, X. C. Li, S. Q. Zhang and J. J. Hou, *Adv. Mater.*, 2013, **25**, 2051–2055.
54 T. Stubhan, N. Li, N. A. Luechinger, S. C. Halim, G. J. Matt and C. J. Brabec, *Adv. Energy Mater.*, 2012, **2**, 1433–1438.
55 S. Bai, M. T. Cao, Y. Z. Jin, X. L. Dai, X. Y. Liang, Z. Z. Ye, M. Li, J. P. Cheng, X. Z. Xiao, Z. W. Wu, Z. H. Xia, B. Q. Sun, E. Wang, Y. Q. Mo, F. Gao and F. L. Zhang, *Adv. Energy Mater.*, 2014, **4**(6), 1301460.
56 H. Liu, J. Tang, I. J. Kramer, R. Debnath, G. I. Koleilat, X. Wang, A. Fisher, R. Li, L. Brzozowski, L. Levina and E. H. Sargent, *Adv. Mater.*, 2011, **23**, 3832–3837.
57 J. A. Ayllon and M. Lira-Cantu, *Appl. Phys. A: Mater. Sci. Process.*, 2008, **95**, 249–255.
58 J. Meyer, S. Hamwi, M. Kroger, W. Kowalsky, T. Riedl and A. Kahn, *Adv. Mater.*, 2012, **24**, 5408–5427.
59 S. Chandra and M. N. Kamalasanan, *Thin Solid Films*, 1996, **288**, 112–115.
60 Y. M. Sun, J. H. Seo, C. J. Takacs, J. Seifter and A. J. Heeger, *Adv. Mater.*, 2011, **23**, 1679–1683.
61 Y. M. Sun, C. J. Takacs, S. R. Cowan, J. H. Seo, X. Gong, A. Roy and A. J. Heeger, *Adv. Mater.*, 2011, **23**, 2226–2230.

62 M. G. Kim, M. G. Kanatzidis, A. Facchetti and T. J. Marks, *Nat. Mater.*, 2011, **10**, 382–388.
63 S. Bai, Z. W. Wu, X. L. Xu, Y. Z. Jin, B. Q. Sun, X. J. Guo, S. S. He, X. Wang, Z. Z. Ye, H. X. Wei, X. Y. Han and W. L. Ma, *Appl. Phys. Lett.*, 2012, **100**, 203906.
64 A. G. Dong, X. C. Ye, J. Chen, Y. J. Kang, T. Gordon, J. M. Kikkawa and C. B. Murray, *J. Am. Chem. Soc.*, 2011, **133**, 998–1006.
65 D. V. Talapin, J. S. Lee, M. V. Kovalenko and E. V. Shevchenko, *Chem. Rev.*, 2010, **110**, 389–458.
66 C. L. Carnes, J. Stipp, K. J. Klabunde and J. Bonevich, *Langmuir*, 2002, **18**, 1352–1359.
67 S. A. El-Safty, M. Khairy, M. Ismael and H. Kawarada, *Appl. Catal., B*, 2012, **123**, 162–173.
68 J. P. Wang and N. C. Greenham, *Appl. Phys. Lett.*, 2014, **104**, 193111.
69 J. Buha, I. Djerdj and M. Niederberger, *Cryst. Growth Des.*, 2007, **7**, 113–116.
70 C. Pacholski, A. Kornowski and H. Weller, *Angew. Chem., Int. Ed.*, 2002, **41**, 1188–1191.
71 P. D. Cozzoli, A. Kornowski and H. Weller, *J. Am. Chem. Soc.*, 2003, **125**, 14539–14548.
72 A. W. Cohn, K. R. Kittilstved and D. R. Gamelin, *J. Am. Chem. Soc.*, 2012, **134**, 7937–7943.
73 X. Wang, X. G. Han, S. F. Xie, Q. Kuang, Y. Q. Jiang, S. B. Zhang, X. L. Mu, G. X. Chen, Z. X. Xie and L. S. Zheng, *Chem. – Eur. J.*, 2012, **18**, 2283–2289.
74 M. Niederberger, M. H. Bard and G. D. Stucky, *J. Am. Chem. Soc.*, 2002, **124**, 13642–13643.
75 Y. F. Chen, M. Kim, G. Lian, M. B. Johnson and X. G. Peng, *J. Am. Chem. Soc.*, 2005, **127**, 13331–13337.
76 J. Polleux, N. Pinna, M. Antonietti and M. Niederberger, *J. Am. Chem. Soc.*, 2005, **127**, 15595–15601.
77 B. H. Wu, C. Y. Guo, N. F. Zheng, Z. X. Xie and G. D. Stucky, *J. Am. Chem. Soc.*, 2008, **130**, 17563–17567.
78 C. T. Dinh, T. D. Nguyen, F. Kleitz and T. O. Do, *ACS Nano*, 2009, **3**, 3737–3743.
79 B. Ludi, M. J. Suess, I. A. Werner and M. Niederberger, *Nanoscale*, 2012, **4**, 1982–1995.
80 G. C. Xi, S. X. Ouyang, P. Li, J. H. Ye, Q. Ma, N. Su, H. Bai and C. Wang, *Angew. Chem., Int. Ed.*, 2012, **51**, 2395–2399.
81 K. Fominykh, J. M. Feckl, J. Sicklinger, M. Doblinger, S. Bocklein, J. Ziegler, L. Peter, J. Rathousky, E. W. Scheidt, T. Bein and D. Fattakhova-Rohlfing, *Adv. Funct. Mater.*, 2014, **24**, 3123–3129.
82 A. Bergerud, R. Buonsanti, J. L. Jordan-Sweet and D. J. Milliron, *Chem. Mater.*, 2013, **25**, 3172–3179.
83 T. R. Gordon, M. Cargnello, T. Paik, F. Mangolini, R. T. Weber, P. Fornasiero and C. B. Murray, *J. Am. Chem. Soc.*, 2012, **134**, 6751–6761.
84 K. Lee, W. S. Seo and J. T. Park, *J. Am. Chem. Soc.*, 2003, **125**, 3408–3409.
85 T. Paik, S. H. Hong, E. A. Gaulding, H. Caglayan, T. R. Gordon, N. Engheta, C. R. Kagan and C. B. Murray, *ACS Nano*, 2014, **8**, 797–806.
86 N. Pinna, G. Garnweitner, M. Antonietti and M. Niederberger, *J. Am. Chem. Soc.*, 2005, **127**, 5608–5612.
87 D. S. Wang, T. Xie, Q. Peng, S. Y. Zhang, J. Chen and Y. D. Li, *Chem. – Eur. J.*, 2008, **14**, 2507–2513.
88 A. Yella, M. N. Tahir, S. Meuer, R. Zentel, R. Berger, M. Panthofer and W. Tremel, *J. Am. Chem. Soc.*, 2009, **131**, 17566–17575.
89 Y. W. Jun, M. F. Casula, J. H. Sim, S. Y. Kim, J. Cheon and A. P. Alivisatos, *J. Am. Chem. Soc.*, 2003, **125**, 15981–15985.
90 T. J. Trentler, T. E. Denler, J. F. Bertone, A. Agrawal and V. L. Colvin, *J. Am. Chem. Soc.*, 1999, **121**, 1613–1614.
91 B. Q. Sun and H. Sirringhaus, *Nano Lett.*, 2005, **5**, 2408–2413.
92 N. Pinna, G. Neri, M. Antonietti and M. Niederberger, *Angew. Chem., Int. Ed.*, 2004, **43**, 4345–4349.
93 I. Bilecka, I. Djerdj and M. Niederberger, *Chem. Commun.*, 2008, 886–888, DOI: 10.1039/b717334b.
94 J. Polleux, A. Gurlo, N. Barsan, U. Weimar, M. Antonietti and M. Niederberger, *Angew. Chem., Int. Ed.*, 2005, **45**, 261–265.
95 I. Olliges-Stadler, J. Stoetzel, D. Koziej, M. D. Rossell, J.-D. Grunwaldt, M. Nachtegaal, R. Frahm and M. Niederberger, *Chem. – Eur. J.*, 2012, **18**, 2305–2312.
96 G. Garnweitner, M. Antonietti and M. Niederberger, *Chem. Commun.*, 2005, 397–399.
97 G. V. Jensen, M. Bremholm, N. Lock, G. R. Deen, T. R. Jensen, B. B. Iversen, M. Niederberger, J. S. Pedersen and H. Birkedal, *Chem. Mater.*, 2010, **22**, 6044–6055.
98 I. Bilecka, P. Elser and M. Niederberger, *ACS Nano*, 2009, **3**, 467–477.
99 Y. F. Yang, Y. Z. Jin, H. P. He, Q. L. Wang, Y. Tu, H. M. Lu and Z. Z. Ye, *J. Am. Chem. Soc.*, 2010, **132**, 13381–13394.
100 X. Y. Liang, Y. P. Ren, S. Bai, N. Zhang, X. L. Dai, X. Wang, H. P. He, C. H. Jin, Z. Z. Ye, Q. Chen, L. W. Chen, J. P. Wang and Y. Z. Jin, *Chem. Mater.*, 2014, **26**, 5169–5178.
101 X. Wang, Y. Z. Jin, H. P. He, F. Yang, Y. F. Yang and Z. Z. Ye, *Nanoscale*, 2013, **5**, 6464–6468.
102 N. Zhang, X. Wang, Z. Z. Ye and Y. Z. Jin, *Sci. Rep.*, 2014, **4**, 04353.
103 A. K. Guria and N. Pradhan, *Chem. Mater.*, 2016, **28**, 5224–5237.
104 N. S. Karan, S. Sarkar, D. D. Sarma, P. Kundu, N. Ravishankar and N. Pradhan, *J. Am. Chem. Soc.*, 2011, **133**, 1666–1669.
105 D. Q. Chen, P. Huang, Y. L. Yu, F. Huang, A. P. Yang and Y. S. Wang, *Chem. Commun.*, 2011, **47**, 5801–5803.
106 R. Buonsanti, A. Llordes, S. Aloni, B. A. Helms and D. J. Milliron, *Nano Lett.*, 2011, **11**, 4706–4710.
107 T. Stubhan, H. Oh, L. Pinna, J. Krantz, I. Litzov and C. J. Brabec, *Org. Electron.*, 2011, **12**, 1539–1543.
108 A. M. Schimpf, S. T. Ochsenbein, R. Buonsanti, D. J. Milliron and D. R. Gamelin, *Chem. Commun.*, 2012, **48**, 9352–9354.
109 E. Della Gaspera, M. Bersani, M. Cittadini, M. Guglielmi, D. Pagani, R. Noriega, S. Mehra, A. Salleo and A. Martucci, *J. Am. Chem. Soc.*, 2013, **135**, 3439–3448.

110 E. Della Gaspera, A. S. R. Chesman, J. van Embden and J. J. Jasieniak, *ACS Nano*, 2014, **8**, 9154–9163.
111 B. L. Greenberg, S. Ganguly, J. T. Held, N. J. Kramer, K. A. Mkhoyan, E. S. Aydil and U. R. Kortshagen, *Nano Lett.*, 2015, **15**, 8162–8169.
112 M. Saha, S. Ghosh, V. D. Ashok and S. K. De, *Phys. Chem. Chem. Phys.*, 2015, **17**, 16067–16079.
113 V. Müller, M. Rasp, G. Štefanić, J. Ba, S. Günther, J. Rathousky, M. Niederberger and D. Fattakhova-Rohlfing, *Chem. Mater.*, 2009, **21**, 5229–5236.
114 L. De Trizio, R. Buonsanti, A. M. Schimpf, A. Llordes, D. R. Gamelin, R. Simonutti and D. J. Milliron, *Chem. Mater.*, 2013, **25**, 3383–3390.
115 Y. J. Liu, J. M. Szeifert, J. M. Feckl, B. Mandlmeier, J. Rathousky, O. Hayden, D. Fattakhova-Rohlfing and T. Bein, *ACS Nano*, 2010, **4**, 5373–5381.
116 R. Buonsanti and D. J. Milliron, *Chem. Mater.*, 2013, **25**, 1305–1317.
117 P. R. Brown, D. Kim, R. R. Lunt, N. Zhao, M. G. Bawendi, J. C. Grossman and V. Bulović, *ACS Nano*, 2014, **8**, 5863–5872.
118 M. L. H. Green, *J. Org. Chem.*, 1995, **500**, 127–148.
119 J. Owen, *Science*, 2015, **347**, 615–616.
120 N. C. Anderson, M. P. Hendricks, J. J. Choi and J. S. Owen, *J. Am. Chem. Soc.*, 2013, **135**, 18536–18548.
121 J. De Roo, I. Van Driessche, J. C. Martins and Z. Hens, *Nat. Mater.*, 2016, **15**, 517–521.
122 J. De Roo, Y. Justo, K. De Keukeleere, F. Van den Broeck, J. C. Martins, I. Van Driessche and Z. Hens, *Angew. Chem., Int. Ed.*, 2015, **54**, 6488–6491.
123 J. De Roo, F. Van den Broeck, K. De Keukeleere, J. C. Martins, I. Van Driessche and Z. Hens, *J. Am. Chem. Soc.*, 2014, **136**, 9650–9657.
124 R. D. Palma, S. Peeters, M. J. Van Bael, H. V. den Rul, K. Bonroy, W. Laureyn, J. Mullens, G. Borghs and G. Maes, *Chem. Mater.*, 2007, **19**, 1821–1831.
125 E. K. U. Larsen, T. Nielsen, T. Wittenborn, H. Birkedal, T. Vorup-Jensen, M. H. Jakobsen, L. Østergaard, M. R. Horsman, F. Besenbacher, K. A. Howard and J. Kjems, *ACS Nano*, 2009, **3**, 1947–1951.
126 R. Gomes, A. Hassinen, A. Szczygiel, Q. Zhao, A. Vantomme, J. C. Martins and Z. Hens, *J. Phys. Chem. Lett.*, 2011, **2**, 145–152.
127 M. V. Kovalenko, M. Scheele and D. V. Talapin, *Science*, 2009, **324**, 1417–1420.
128 D. C. Oertel, M. G. Bawendi, A. C. Arango and V. Bulovic, *Appl. Phys. Lett.*, 2005, **87**, 213505.
129 M. V. Kovalenko, M. I. Bodnarchuk and D. V. Talapin, *J. Am. Chem. Soc.*, 2010, **132**, 15124–15126.
130 A. W. Wills, M. S. Kang, A. Khare, W. L. Gladfelter and D. J. Norris, *ACS Nano*, 2010, **4**, 4523–4530.
131 M. V. Kovalenko, M. I. Bodnarchuk, J. Zaumseil, J.-S. Lee and D. V. Talapin, *J. Am. Chem. Soc.*, 2010, **132**, 10085–10092.
132 Y. Yang, H. Y. Qin, M. W. Jiang, L. Lin, T. Fu, X. L. Dai, Z. Z. Zhang, Y. Niu, H. J. Cao, Y. Z. Jin, F. Zhao and X. G. Peng, *Nano Lett.*, 2016, **16**, 2133–2138.
133 Y. Yang, H. Y. Qin and X. G. Peng, *Nano Lett.*, 2016, **16**, 2127–2132.
134 J. P. Wang, *Optoelectronic Properties and Memory Effects of ZnO Nanocrystals*, University of Cambridge, 2009.
135 L. S. M. Hilgendorff, C. Rothenhöusler and G. Muller, *J. Electrochem. Soc.*, 1998, **145**, 3632–3637.
136 S. Y. Liu, R. Liu, Y. Chen, S. Ho, J. H. Kim and F. So, *Chem. Mater.*, 2014, **26**, 4528–4534.
137 J. Zhang, J. T. Wang, Y. Y. Fu, B. H. Zhang and Z. Y. Xie, *J. Mater. Chem. C*, 2014, **2**, 8295–8302.
138 Y. H. Zhou, C. Fuentes-Hernandez, J. Shim, J. Meyer, A. J. Giordano, H. Li, P. Winget, T. Papadopoulos, H. Cheun, J. Kim, M. Fenoll, A. Dindar, W. Haske, E. Najafabadi, T. M. Khan, H. Sojoudi, S. Barlow, S. Graham, J. L. Bredas, S. R. Marder, A. Kahn and B. Kippelen, *Science*, 2012, **336**, 327–332.
139 Y. E. Ha, M. Y. Jo, J. Park, Y.-C. Kang, S. II. Yoo and J. H. Kim, *J. Phys. Chem. C*, 2013, **117**, 2646–2652.
140 Q. B. Pei and Y. Yang, *J. Am. Chem. Soc.*, 1996, **118**, 7416–7417.
141 H. J. Bolink, E. Coronado, D. Repetto and M. Sessolo, *Appl. Phys. Lett.*, 2007, **91**, 223501.
142 N. Aizawa, Y. J. Pu, M. Watanabe, T. Chiba, K. Ideta, N. Toyota, M. Igarashi, Y. Suzuri, H. Sasabe and J. Kido, *Nat. Commun.*, 2014, **5**, 5756.
143 M. Cai, T. Xiao, E. Hellerich, Y. Chen, R. Shinar and J. Shinar, *Adv. Mater.*, 2011, **23**, 3590–3596.
144 L. Ying, C. L. Ho, H. B. Wu, Y. Cao and W. Y. Wong, *Adv. Mater.*, 2014, **26**, 2459–2473.
145 M. Sessolo and H. J. Bolink, *Adv. Mater.*, 2011, **23**, 1829–1845.
146 S. A. Haque, S. Koops, N. Tokmoldin, J. R. Durrant, J. Huang, D. D. C. Bradley and E. Palomares, *Adv. Mater.*, 2007, **19**, 683–687.
147 L. Qian, Y. Zheng, K. R. Choudhury, D. Bera, F. So, J. G. Xue and P. H. Holloway, *Nano Today*, 2010, **5**, 384–389.
148 M. Sessolo, H. J. Bolink, H. Brine, H. Prima-Garcia and R. Tena-Zaera, *J. Mater. Chem.*, 2012, **22**, 4916.
149 E. F. Schubert, T. Gessmann and J. K. Kim, *Light Emitting Diodes*, John Wiley & Sons, Inc., 2005.
150 T. Chiba, Y.-J. Pu, H. Sasabe, J. Kido and Y. Yang, *J. Mater. Chem.*, 2012, **22**, 22769.
151 T. Chiba, Y.-J. Pu and J. Kido, *Adv. Mater.*, 2015, **27**, 4681–4687.
152 M. Zhang, S. Hofle, J. Czolk, A. Mertens and A. Colsmann, *Nanoscale*, 2015, **7**, 20009–20014.
153 S. Höfle, A. Schienle, C. Bernhard, M. Bruns, U. Lemmer and A. Colsmann, *Adv. Mater.*, 2014, **26**, 5155–5159.
154 Y.-J. Pu, T. Chiba, K. Ideta, S. Takahashi, N. Aizawa, T. Hikichi and J. Kido, *Adv. Mater.*, 2015, **27**, 1327–1332.
155 H. Lee, C.-M. Kang, M. Park, J. Kwak and C. Lee, *ACS Appl. Mater. Interfaces*, 2013, **5**, 1977–1981.
156 J. Meyer, R. Khalandovsky, P. Görrn and A. Kahn, *Adv. Mater.*, 2011, **23**, 70–73.
157 G. J. Supran, Y. Shirasaki, K. W. Song, J.-M. Caruge, P. T. Kazlas, S. Coe-Sullivan, T. L. Andrew, M. G. Bawendi and V. Bulovic, *MRS Bull.*, 2013, **38**, 703–711.

158 J. M. Pietryga, Y.-S. Park, J. Lim, A. F. Fidler, W. K. Bae, S. Brovelli and V. I. Klimov, *Chem. Rev.*, 2016, **116**, 10513–10622.
159 V. L. Colvin, M. C. Schlamp and A. P. Alivisatos, *Nature*, 1994, **370**, 354–357.
160 B. O. Dabbousi, M. G. Bawendi, O. Onitsuka and M. F. Rubner, *Appl. Phys. Lett.*, 1995, **66**, 1316–1318.
161 M. C. Schlamp, X. G. Peng and A. P. Alivisatos, *J. Appl. Phys.*, 1997, **82**, 5837–5842.
162 S. Coe, W. K. Woo, M. Bawendi and V. Bulović, *Nature*, 2002, **420**, 800–803.
163 S. Coe-Sullivan, W. K. Woo, J. S. Steckel, M. Bawendi and V. Bulovic, *Org. Electron.*, 2003, **4**, 123–130.
164 S. Coe-Sullivan, J. S. Steckel, W. K. Woo, M. G. Bawendi and V. Bulovic, *Adv. Funct. Mater.*, 2005, **15**, 1117–1124.
165 J. S. Steckel, P. Snee, S. Coe-Sullivan, J. P. Zimmer, J. E. Halpert, P. Anikeeva, L. A. Kim, V. Bulovic and M. G. Bawendi, *Angew. Chem., Int. Ed.*, 2006, **45**, 5796–5799.
166 P. O. Anikeeva, J. E. Halpert, M. G. Bawendi and V. Bulovic, *Nano Lett.*, 2007, **7**, 2196–2200.
167 Y. H. Niu, A. M. Munro, Y. J. Cheng, Y. Tian, M. S. Liu, J. Zhao, J. A. Bardecker, I. Jen-La Plante, D. S. Ginger and A. K. Y. Jen, *Adv. Mater.*, 2007, **19**, 3371–3376.
168 P. O. Anikeeva, C. F. Madigan, J. E. Halpert, M. G. Bawendi and V. Bulovic, *Phys. Rev. B: Condens. Matter Mater. Phys.*, 2008, **78**, 085434.
169 P. O. Anikeeva, J. E. Halpert, M. G. Bawendi and V. Bulovic, *Nano Lett.*, 2009, **9**, 2532–2536.
170 Q. J. Sun, G. Subramanyam, L. M. Dai, M. Check, A. Campbell, R. Naik, J. Grote and Y. Q. Wang, *ACS Nano*, 2009, **3**, 737–743.
171 L. Qian, Y. Zheng, J. G. Xue and P. H. Holloway, *Nat. Photonics*, 2011, **5**, 543–548.
172 J. Kwak, W. K. Bae, D. Lee, I. Park, J. Lim, M. Park, H. Cho, H. Woo, D. Y. Yoon, K. Char, S. Lee and C. Lee, *Nano Lett.*, 2012, **12**, 2362–2366.
173 K.-H. Lee, J.-H. Lee, W.-S. Song, H. Ko, C. Lee, J.-H. Lee and H. Yang, *ACS Nano*, 2013, **7**, 7295–7302.
174 K.-H. Lee, J.-H. Lee, H.-D. Kang, B. Park, Y. Kwon, H. Ko, C. Lee, J. Lee and H. Yang, *ACS Nano*, 2014, **8**, 4893–4901.
175 H. B. Shen, W. R. Cao, N. T. Shewmon, C. C. Yang, L. S. Li and J. G. Xue, *Nano Lett.*, 2015, **15**, 1211–1216.
176 Y. Gao and X. G. Peng, *J. Am. Chem. Soc.*, 2015, **137**, 4230–4235.
177 C. D. Pu and X. G. Peng, *J. Am. Chem. Soc.*, 2016, **138**, 8134–8142.
178 Z. A. Peng and X. G. Peng, *J. Am. Chem. Soc.*, 2002, **124**, 3343–3353.
179 O. Chen, J. Zhao, V. P. Chauhan, J. Cui, C. Wong, D. K. Harris, H. Wei, H.-S. Han, D. Fukumura and R. K. Jain, *Nat. Mater.*, 2013, **12**, 445–451.
180 W. E. Ford, D. Gao, N. Knorr, R. Wirtz, F. Scholz, Z. Karipidou, K. Ogasawara, S. Rosselli, V. Rodin, G. Nelles and F. von Wrochem, *ACS Nano*, 2014, **8**, 9173–9180.
181 J. M. Caruge, J. E. Halpert, V. Wood, V. Bulović and M. G. Bawendi, *Nat. Photonics*, 2008, **2**, 247–250.
182 J. W. Stouwdam and R. A. J. Janssen, *J. Mater. Chem.*, 2008, **18**, 1889–1894.
183 J.-M. C. Yajie Dong, Z. Zhou, C. Hamilton, J. H. Zoran Popovic, M. Stevenson, G. Liu, V. Bulovic, M. Bawendi, P. T. Kazlas, J. Steckel and S. Coe-Sullivan, *SID Int. Symp. Dig. Tech. Pap.*, 2015, **46**, 270–273.
184 H. Zhang, N. Sui, X. Chi, Y. Wang, Q. Liu, H. Zhang and W. Ji, *ACS Appl. Mater. Interfaces*, 2016, **8**, 31385–31391.
185 J.-H. Kim, C.-Y. Han, K.-H. Lee, K.-S. An, W. Song, J. Kim, M. S. Oh, Y. R. Do and H. Yang, *Chem. Mater.*, 2015, **27**, 197–204.
186 H. T. Nguyen, N. D. Nguyen and S. Lee, *Nanotechnology*, 2013, **24**, 115201.
187 H. T. Nguyen, H. Jeong, J.-Y. Park, Y. H. Ahn and S. Lee, *ACS Appl. Mater. Interfaces*, 2014, **6**, 7286–7291.
188 T. Ding, X. Y. Yang, L. Y. Bai, Y. B. Zhao, K. E. Fong, N. Wang, H. V. Demir and X. W. Sun, *Org. Electron.*, 2015, **26**, 245–250.
189 X. Y. Yang, Y. Y. Ma, E. Mutlugun, Y. B. Zhao, K. S. Leck, S. T. Tan, H. V. Demir, Q. Y. Zhang, H. J. Du and X. W. Sun, *ACS Appl. Mater. Interfaces*, 2014, **6**, 495–499.
190 S. Bhaumik and A. J. Pal, *ACS Appl. Mater. Interfaces*, 2014, **6**, 11348–11356.
191 F. Deschler, M. Price, S. Pathak, L. E. Klintberg, D. D. Jarausch, R. Higler, S. Huttner, T. Leijtens, S. D. Stranks, H. J. Snaith, M. Atature, R. T. Phillips and R. H. Friend, *J. Phys. Chem. Lett.*, 2014, **5**, 1421–1426.
192 Z. K. Tan, R. S. Moghaddam, M. L. Lai, P. Docampo, R. Higler, F. Deschler, M. Price, A. Sadhanala, L. M. Pazos, D. Credgington, F. Hanusch, T. Bein, H. J. Snaith and R. H. Friend, *Nat. Nanotechnol.*, 2014, **9**, 687–692.
193 J. P. Wang, N. N. Wang, Y. Z. Jin, J. J. Si, Z. K. Tan, H. Du, L. Cheng, X. L. Dai, S. Bai, H. P. He, Z. Z. Ye, M. L. Lai, R. H. Friend and W. Huang, *Adv. Mater.*, 2015, **27**, 2311–2316.
194 M. Yuan, L. N. Quan, R. Comin, G. Walters, R. Sabatini, O. Voznyy, S. Hoogland, Y. Zhao, E. M. Beauregard and P. Kanjanaboos, *Nat. Nanotechnol.*, 2016, 872–877.
195 H. Cho, S.-H. Jeong, M.-H. Park, Y.-H. Kim, C. Wolf, C.-L. Lee, J. H. Heo, A. Sadhanala, N. Myoung and S. Yoo, *Science*, 2015, **350**, 1222–1225.
196 G. Li, V. Shrotriya, J. S. Huang, Y. Yao, T. Moriarty, K. Emery and Y. Yang, *Nat. Mater.*, 2005, **4**, 864–868.
197 S. H. Park, A. Roy, S. Beaupré, S. Cho, N. Coates, J. S. Moon, D. Moses, M. Leclerc, K. Lee and A. J. Heeger, *Nat. Photonics*, 2009, **3**, 297–302.
198 Z. C. He, C. M. Zhong, S. J. Su, M. Xu, H. B. Wu and Y. Cao, *Nat. Photonics*, 2012, **6**, 591–595.
199 S. Li, L. Ye, W. Zhao, S. Zhang, S. Mukherjee, H. Ade and J. Hou, *Adv. Mater.*, 2016, **28**, 9423–9429.
200 J. Zhao, Y. Li, G. Yang, K. Jiang, H. Lin, H. Ade, W. Ma and H. Yan, *Nat. Energy*, 2016, **1**, 15027.
201 J. Peet, J. Y. Kim, N. E. Coates, W. L. Ma, D. Moses, A. J. Heeger and G. C. Bazan, *Nat. Mater.*, 2007, **6**, 497–500.
202 W. C. Zhao, D. P. Qian, S. Q. Zhang, S. S. Li, O. Inganäs, F. Gao and J. H. Hou, *Adv. Mater.*, 2016, **28**, 4734–4739.
203 Y. Li, *Acc. Chem. Res.*, 2012, **45**, 723–733.

204 Y. Z. Lin, F. W. Zhao, Q. He, L. J. Huo, Y. Wu, T. C. Parker, W. Ma, Y. M. Sun, C. R. Wang and D. B. Zhu, *J. Am. Chem. Soc.*, 2016, **138**, 4955–4961.
205 J. Y. Kim, K. Lee, N. E. Coates, D. Moses, T.-Q. Nguyen, M. Dante and A. J. Heeger, *Science*, 2007, **317**, 222–225.
206 A. K. K. Kyaw, X. W. Sun, C. Y. Jiang, G. Q. Lo, D. W. Zhao and D. L. Kwong, *Appl. Phys. Lett.*, 2008, **93**, 221107.
207 W. J. E. Beek, M. M. Wienk, M. Kemerink, X. N. Yang and R. A. J. Janssen, *J. Phys. Chem. B*, 2005, **109**, 9505–9516.
208 M.-H. Park, J.-H. Li, A. Kumar, G. Li and Y. Yang, *Adv. Funct. Mater.*, 2009, **19**, 1241–1246.
209 F. J. Lim, K. Ananthanarayanan, J. Luther and G. W. Ho, *J. Mater. Chem.*, 2012, **22**, 25057.
210 H. Schmidt, K. Zilberberg, S. Schmale, H. Flügge, T. Riedl and W. Kowalsky, *Appl. Phys. Lett.*, 2010, **96**, 243305.
211 F.-X. Xie, W. C. H. Choy, W. E. I. Sha, D. Zhang, S. Zhang, X. Li, C.-W. Leung and J. Hou, *Energy Environ. Sci.*, 2013, **6**, 3372.
212 D. Zhang, W. C. H. Choy, F. Xie, W. E. I. Sha, X. C. Li, B. F. Ding, K. Zhang, F. Huang and Y. Cao, *Adv. Funct. Mater.*, 2013, **23**, 4255–4261.
213 J. B. You, C.-C. Chen, L. T. Dou, S. Murase, H.-S. Duan, S. A. Hawks, T. Xu, H. J. Son, L. P. Yu, G. Li and Y. Yang, *Adv. Mater.*, 2012, **24**, 5267–5272.
214 S. K. Hau, H.-L. Yip, N. S. Baek, J. Zou, K. O'Malley and A. K.-Y. Jen, *Appl. Phys. Lett.*, 2008, **92**, 253301.
215 M. Gaceur, S. B. Dkhil, D. Duché, F. Bencheikh, J.-J. Simon, L. Escoubas, M. Mansour, A. Guerrero, G. Garcia-Belmonte, X. Liu, M. Fahlman, W. Dachraoui, A. K. Diallo, C. Videlot-Ackermann, O. Margeat and J. Ackermann, *Adv. Funct. Mater.*, 2016, **26**, 243–253.
216 R. M. Hewlett and M. A. McLachlan, *Adv. Mater.*, 2016, **28**, 3893–3921.
217 Z. Q. Liang, Q. F. Zhang, L. Jiang and G. Z. Cao, *Energy Environ. Sci.*, 2015, **8**, 3442–3476.
218 S. B. Dkhil, D. Duché, M. Gaceur, A. K. Thakur, F. B. Aboura, L. Escoubas, J.-J. Simon, A. Guerrero, J. Bisquert, G. Garcia-Belmonte, Q. Y. Bao, M. Fahlman, C. Videlot-Ackermann, O. Margeat and J. Ackermann, *Adv. Energy Mater.*, 2014, **4**, 1400805.
219 J. B. You, L. Dou, K. Yoshimura, T. Kato, K. Ohya, T. Moriarty, K. Emery, C.-C. Chen, J. Gao, G. Li and Y. Yang, *Nat. Commun.*, 2013, **4**, 1446.
220 J. Y. Yuan, J. N. Gu, G. Z. Shi, J. X. Sun, H. Q. Wang and W. L. Ma, *Sci. Rep.*, 2016, **6**, 26459.
221 L. T. Dou, J. B. You, J. Yang, C.-C. Chen, Y. J. He, S. Murase, T. Moriarty, K. Emery, G. Li and Y. Yang, *Nat. Photonics*, 2012, **6**, 180–185.
222 T. Ameri, G. Dennler, C. Lungenschmied and C. J. Brabec, *Energy Environ. Sci.*, 2009, **2**, 347–363.
223 C.-C. Chen, W.-H. Chang, K. Yoshimura, K. Ohya, J. B. You, J. Gao, Z. R. Hong and Y. Yang, *Adv. Mater.*, 2014, **26**, 5670–5677.
224 J. Jo, J.-R. Pouliot, D. Wynands, S. D. Collins, J. Y. Kim, T. L. Nguyen, H. Y. Woo, Y. M. Sun, M. Leclerc and A. J. Heeger, *Adv. Mater.*, 2013, **25**, 4783–4788.
225 H. Q. Zhou, Y. Zhang, C.-K. Mai, S. D. Collins, G. C. Bazan, T.-Q. Nguyen and A. J. Heeger, *Adv. Mater.*, 2015, **27**, 1767–1773.
226 A. Gadisa, Y. Liu, E. T. Samulski and R. Lopez, *Appl. Phys. Lett.*, 2012, **100**, 253903.
227 S. Chen, C. E. Small, C. M. Amb, J. Subbiah, T.-h. Lai, S.-W. Tsang, J. R. Manders, J. R. Reynolds and F. So, *Adv. Energy Mater.*, 2012, **2**, 1333–1337.
228 M. Prosa, M. Tessarolo, M. Bolognesi, O. Margeat, D. Gedefaw, M. Gaceur, C. Videlot-Ackermann, M. R. Andersson, M. Muccini, M. Seri and J. Ackermann, *ACS Appl. Mater. Interfaces*, 2016, **8**, 1635–1643.
229 S. Trost, T. Becker, A. Polywka, P. Görrn, M. F. Oszajca, N. A. Luechinger, D. Rogalla, M. Weidner, P. Reckers, T. Mayer and T. Riedl, *Adv. Energy Mater.*, 2016, **6**, 1600347.
230 S. K. Hau, H.-L. Yip, H. Ma and A. K.-Y. Jen, *Appl. Phys. Lett.*, 2008, **93**, 233304.
231 S. Y. Shao, K. B. Zheng, T. Pullerits and F. L. Zhang, *ACS Appl. Mater. Interfaces*, 2013, **5**, 380–385.
232 S. B. Jo, J. H. Lee, M. Sim, M. Kim, J. H. Park, Y. S. Choi, Y. Kim, S.-G. Ihn and K. Cho, *Adv. Energy Mater.*, 2011, **1**, 690–698.
233 T. Hu, F. Li, K. Yuan and Y. W. Chen, *ACS Appl. Mater. Interfaces*, 2013, **5**, 5763–5770.
234 Y.-J. Lee, J. Yi, G. F. Gao, H. Koerner, K. Park, J. Wang, K. Y. Luo, R. A. Vaia and J. W. P. Hsu, *Adv. Energy Mater.*, 2012, **2**, 1193–1197.
235 T. Stubhan, N. Li, N. A. Luechinger, S. C. Halim, G. J. Matt and C. J. Brabec, *Adv. Energy Mater.*, 2012, **2**, 1433–1438.
236 J.-S. Huang, C.-Y. Chou and C.-F. Lin, *IEEE Electron Device Lett.*, 2010, **31**, 332–334.
237 P. Schulz, S. R. Cowan, Z.-L. Guan, A. Garcia, D. C. Olson and A. Kahn, *Adv. Funct. Mater.*, 2014, **24**, 701–706.
238 Z. C. Zhai, X. D. Huang, M. F. Xu, J. Y. Yuan, J. Peng and W. L. Ma, *Adv. Energy Mater.*, 2013, **3**, 1614–1622.
239 D. A. Barkhouse, R. Debnath, I. J. Kramer, D. Zhitomirsky, A. G. Pattantyus-Abraham, L. Levina, L. Etgar, M. Gratzel and E. H. Sargent, *Adv. Mater.*, 2011, **23**, 3134–3138.
240 L. Etgar, D. Yanover, R. K. Čapek, R. Vaxenburg, Z. S. Xue, B. Liu, M. K. Nazeeruddin, E. Lifshitz and M. Grätzel, *Adv. Funct. Mater.*, 2013, **23**, 2736–2741.
241 A. G. Pattantyus-Abraham, I. J. Kramer, A. R. Barkhouse, X. H. Wang, G. Konstantatos, R. Debnath, L. Levina, I. Raabe, M. K. Nazeeruddin, M. Gratzel and E. H. Sargent, *ACS Nano*, 2010, **4**, 3374–3380.
242 M. L. Bohm, T. C. Jellicoe, M. Tabachnyk, N. J. Davis, F. Wisnivesky-Rocca-Rivarola, C. Ducati, B. Ehrler, A. A. Bakulin and N. C. Greenham, *Nano Lett.*, 2015, **15**, 7987–7993.
243 D. A. Barkhouse, A. G. Pattantyus-Abraham, L. Levina and E. H. Sargent, *ACS Nano*, 2008, **2**, 2356–2362.
244 G. I. Koleilat, L. Levina, H. Shukla, S. H. Myrskog, S. Hinds, A. G. Pattantyus-Abraham and E. H. Sargent, *ACS Nano*, 2008, **2**, 833–840.
245 J. M. Luther, M. Law, M. C. Beard, Q. Song, M. O. Reese, R. J. Ellingson and A. J. Nozik, *Nano Lett.*, 2008, **8**, 3488–3492.

246 J. Tang, X. H. Wang, L. Brzozowski, D. A. Barkhouse, R. Debnath, L. Levina and E. H. Sargent, *Adv. Mater.*, 2010, **22**, 1398–1402.
247 A. H. Ip, S. M. Thon, S. Hoogland, O. Voznyy, D. Zhitomirsky, R. Debnath, L. Levina, L. R. Rollny, G. H. Carey, A. Fischer, K. W. Kemp, I. J. Kramer, Z. Ning, A. J. Labelle, K. W. Chou, A. Amassian and E. H. Sargent, *Nat. Nanotechnol.*, 2012, **7**, 577–582.
248 J. J. Choi, Y.-F. Lim, M. B. Santiago-Berrios, M. Oh, B. R. Hyun, L. F. Sun, A. C. Bartnik, A. Goedhart, G. G. Malliaras, H. D. Abruna, F. W. Wise and T. Hanrath, *Nano Lett.*, 2009, **9**, 3749–3755.
249 J. M. Luther, J. Gao, M. T. Lloyd, O. E. Semonin, M. C. Beard and A. J. Nozik, *Adv. Mater.*, 2010, **22**, 3704–3707.
250 J. Tang, K. W. Kemp, S. Hoogland, K. S. Jeong, H. Liu, L. Levina, M. Furukawa, X. H. Wang, R. Debnath, D. Cha, K. W. Chou, A. Fischer, A. Amassian, J. B. Asbury and E. H. Sargent, *Nat. Mater.*, 2011, **10**, 765–771.
251 C. H. Chuang, P. R. Brown, V. Bulovic and M. G. Bawendi, *Nat. Mater.*, 2014, **13**, 796–801.
252 X. Z. Lan, O. Voznyy, A. Kiani, F. P. Garcia de Arquer, A. S. Abbas, G. H. Kim, M. X. Liu, Z. Y. Yang, G. Walters, J. X. Xu, M. J. Yuan, Z. J. Ning, F. J. Fan, P. Kanjanaboos, I. Kramer, D. Zhitomirsky, P. Lee, A. Perelgut, S. Hoogland and E. H. Sargent, *Adv. Mater.*, 2016, **28**, 299–304.
253 Z. J. Ning, Y. Ren, S. Hoogland, O. Voznyy, L. Levina, P. Stadler, X. Z. Lan, D. Zhitomirsky and E. H. Sargent, *Adv. Mater.*, 2012, **24**, 6295–6299.
254 M. Liu, F. P. de Arquer, Y. Li, X. Lan, G. H. Kim, O. Voznyy, L. K. Jagadamma, A. S. Abbas, S. Hoogland, Z. Lu, J. Y. Kim, A. Amassian and E. H. Sargent, *Adv. Mater.*, 2016, **28**, 4142–4148.
255 K. W. Kemp, A. J. Labelle, S. M. Thon, A. H. Ip, I. J. Kramer, S. Hoogland and E. H. Sargent, *Adv. Energy Mater.*, 2013, **3**, 917–922.
256 S. M. Willis, C. Cheng, H. E. Assender and A. A. Watt, *Nano Lett.*, 2012, **12**, 1522–1526.
257 X. H. Wang, G. I. Koleilat, A. Fischer, J. Tang, R. Debnath, L. Levina and E. H. Sargent, *ACS Appl. Mater. Interfaces*, 2011, **3**, 3792–3795.
258 B. Ehrler, K. P. Musselman, M. L. Bohm, F. S. Morgenstern, Y. Vaynzof, B. J. Walker, J. L. Macmanus-Driscoll and N. C. Greenham, *ACS Nano*, 2013, **7**, 4210–4220.
259 R. Azmi, S.-H. Oh and S.-Y. Jang, *ACS Energy Lett.*, 2016, **1**, 100–106.
260 A. Kojima, K. Teshima, Y. Shirai and T. Miyasaka, *J. Am. Chem. Soc.*, 2009, **131**, 6050–6051.
261 W. Zhang, G. E. Eperon and H. J. Snaith, *Nat. Energy*, 2016, **1**, 16048.
262 H.-S. Kim, C.-R. Lee, J.-H. Im, K.-B. Lee, T. Moehl, A. Marchioro, S.-J. Moon, R. Humphry-Baker, J.-H. Yum, J. E. Moser, M. Grätzel and N.-G. Park, *Sci. Rep.*, 2012, **2**, 591.
263 H. P. Zhou, Q. Chen, G. Li, S. Luo, T.-b. Song, H.-S. Duan, Z. R. Hong, J. B. You, Y. S. Liu and Y. Yang, *Science*, 2014, **345**, 542.
264 W. S. Yang, J. H. Noh, N. J. Jeon, Y. C. Kim, S. Ryu, J. Seo and S. I. Seok, *Science*, 2015, **348**, 1234–1237.
265 N. J. Jeon, J. H. Noh, Y. C. Kim, W. S. Yang, S. Ryu and S. I. Seok, *Nat. Mater.*, 2014, **13**, 897–903.
266 N. J. Jeon, J. H. Noh, W. S. Yang, Y. C. Kim, S. Ryu, J. Seo and S. I. Seok, *Nature*, 2015, **517**, 476–480.
267 D. P. McMeekin, G. Sadoughi, W. Rehman, G. E. Eperon, M. Saliba, M. T. Horantner, A. Haghighirad, N. Sakai, L. Korte, B. Rech, M. B. Johnston, L. M. Herz and H. J. Snaith, *Science*, 2016, **351**, 151–155.
268 H. Tsai, W. Y. Nie, J. C. Blancon, C. C. Stoumpos, R. Asadpour, B. Harutyunyan, A. J. Neukirch, R. Verduzco, J. J. Crochet, S. Tretiak, L. Pedesseau, J. Even, M. A. Alam, G. Gupta, J. Lou, P. M. Ajayan, M. J. Bedzyk and M. G. Kanatzidis, *Nature*, 2016, **536**, 312–316.
269 J. Burschka, N. Pellet, S.-J. Moon, R. Humphry-Baker, P. Gao, M. K. Nazeeruddin and M. Gratzel, *Nature*, 2013, **499**, 316–319.
270 S. D. Stranks, G. E. Eperon, G. Grancini, C. Menelaou, M. J. P. Alcocer, T. Leijtens, L. M. Herz, A. Petrozza and H. J. Snaith, *Science*, 2013, **342**, 341.
271 G. C. Xing, N. Mathews, S. Y. Sun, S. S. Lim, Y. M. Lam, M. Grätzel, S. Mhaisalkar and T. C. Sum, *Science*, 2013, **342**, 344–347.
272 M. Z. Liu, M. B. Johnston and H. J. Snaith, *Nature*, 2013, **501**, 395–398.
273 J.-Y. Jeng, Y.-F. Chiang, M.-H. Lee, S.-R. Peng, T.-F. Guo, P. Chen and T.-C. Wen, *Adv. Mater.*, 2013, **25**, 3727–3732.
274 S. Bai, N. Sakai, W. Zhang, Z. Wang, J. T. W. Wang, F. Gao and H. J. Snaith, *Chem. Mater.*, 2017, **29**, 462–473.
275 D. Liu and T. L. Kelly, *Nat. Photonics*, 2014, **8**, 133–138.
276 J. P. Correa Baena, L. Steier, W. Tress, M. Saliba, S. Neutzner, T. Matsui, F. Giordano, T. J. Jacobsson, A. R. Srimath Kandada, S. M. Zakeeruddin, A. Petrozza, A. Abate, M. K. Nazeeruddin, M. Gratzel and A. Hagfeldt, *Energy Environ. Sci.*, 2015, **8**, 2928–2934.
277 S. S. Shin, W. S. Yang, J. H. Noh, J. H. Suk, N. J. Jeon, J. H. Park, J. S. Kim, W. M. Seong and S. I. Seok, *Nat. Commun.*, 2015, **6**, 8410.
278 H. S. Rao, B. X. Chen, W. G. Li, Y. F. Xu, H. Y. Chen, D. B. Kuang and C. Y. Su, *Adv. Funct. Mater.*, 2015, **25**, 7200–7207.
279 S. S. Shin, W. S. Yang, E. J. Yeom, S. J. Lee, N. J. Jeon, Y.-C. Joo, I. J. Park, J. H. Noh and S. I. Seok, *J. Phys. Chem. Lett.*, 2016, **7**, 1845–1851.
280 T. Leijtens, G. E. Eperon, S. Pathak, A. Abate, M. M. Lee and H. J. Snaith, *Nat. Commun.*, 2013, **4**, 2885.
281 H. J. Snaith, A. Abate, J. M. Ball, G. E. Eperon, T. Leijtens, N. K. Noel, S. D. Stranks, J. T.-W. Wang, K. Wojciechowski and W. Zhang, *J. Phys. Chem. Lett.*, 2014, **5**, 1511–1515.
282 Y. Zhang, M. Z. Liu, G. E. Eperon, T. C. Leijtens, D. McMeekin, M. Saliba, W. Zhang, M. de Bastiani, A. Petrozza, L. M. Herz, M. B. Johnston, H. Lin and H. J. Snaith, *Mater. Horiz.*, 2015, **2**, 315–322.
283 Y. C. Shao, Z. G. Xiao, C. Bi, Y. B. Yuan and J. S. Huang, *Nat. Commun.*, 2014, **5**, 5784.

284 P. Docampo, J. M. Ball, M. Darwich, G. E. Eperon and H. J. Snaith, *Nat. Commun.*, 2013, **4**, 2761.
285 Z. L. Zhu, Y. Bai, X. Liu, C.-C. Chueh, S. H. Yang and A. K. Y. Jen, *Adv. Mater.*, 2016, **28**, 6478–6484.
286 A. Savva, I. Burgués-Ceballos and S. A. Choulis, *Adv. Energy Mater.*, 2016, **6**, 1600285.
287 X. Liu, C.-C. Chueh, Z. L. Zhu, S. B. Jo, Y. Sun and A. K. Y. Jen, *J. Mater. Chem. A*, 2016, **4**, 15294–15301.
288 K. A. Bush, C. D. Bailie, Y. Chen, A. R. Bowring, W. Wang, W. Ma, T. Leijtens, F. Moghadam and M. D. McGehee, *Adv. Mater.*, 2016, **28**, 3937–3943.
289 W. H. Sun, Y. L. Li, S. Y. Ye, H. X. Rao, W. B. Yan, H. T. Peng, Y. Li, Z. W. Liu, S. F. Wang, Z. J. Chen, L. X. Xiao, Z. Q. Bian and C. H. Huang, *Nanoscale*, 2016, **8**, 10806–10813.
290 H. X. Rao, S. Y. Ye, W. H. Sun, W. Yan, Y. L. Li, H. T. Peng, Z. W. Liu, Z. Q. Bian, Y. F. Li and C. H. Huang, *Nano Energy*, 2016, **27**, 51–57.
291 Z.-L. Tseng, L.-C. Chen, C.-H. Chiang, S.-H. Chang, C.-C. Chen and C.-G. Wu, *Sol. Energy*, 2016, **139**, 484–488.
292 H. C. Sun, X. M. Hou, Q. L. Wei, H. W. Liu, K. C. Yang, W. Wang, Q. Y. An and Y. G. Rong, *Chem. Commun.*, 2016, **52**, 8099–8102.
293 H. Back, G. Kim, J. Kim, J. Kong, T. K. Kim, H. Kang, H. Kim, J. Lee, S. Lee and K. Lee, *Energy Environ. Sci.*, 2016, **9**, 1258–1263.
294 J. N. You, L. Meng, T. B. Song, T. F. Guo, Y. M. Yang, W. H. Chang, Z. R. Hong, H. J. Chen, H. P. Zhou, Q. Chen, Y. S. Liu, N. De Marco and Y. Yang, *Nat. Nanotechnol.*, 2016, **11**, 75–81.
295 X. T. Yin, P. Chen, M. D. Que, Y. L. Xing, W. X. Que, C. M. Niu and J. Y. Shao, *ACS Nano*, 2016, **10**, 3630–3636.
296 H. Zhang, J. Q. Cheng, F. Lin, H. X. He, J. Mao, K. S. Wong, A. K. Jen and W. C. Choy, *ACS Nano*, 2016, **10**, 1503–1511.